January 2016

Determining Fuel Type from Estimates of Bulk Modulus Using Rail Pressure Measurements

Mukta Vijay Kulkarni
Purdue University

PURDUE UNIVERSITY
GRADUATE SCHOOL
Thesis/Dissertation Acceptance

This is to certify that the thesis/dissertation prepared

By Mukta Vijay Kulkarni

Entitled

Determine Fuel Type from Estimates of Bulk Modulus Using Rail Pressure Measurements

For the degree of Master of Science in Mechanical Engineering

Is approved by the final examining committee:

Dr. Peter H. Meckl
Chair

Dr. Gregory M. Shaver

Dr. Patricia Davies

To the best of my knowledge and as understood by the student in the Thesis/Dissertation Agreement, Publication Delay, and Certification Disclaimer (Graduate School Form 32), this thesis/dissertation adheres to the provisions of Purdue University's "Policy of Integrity in Research" and the use of copyright material.

Approved by Major Professor(s): Dr. Peter H. Meckl

Approved by: Dr. Jay P. Gore 12/1/2016

Head of the Departmental Graduate Program Date

DETERMINING FUEL TYPE FROM ESTIMATES OF BULK MODULUS USING RAIL PRESSURE MEASUREMENTS

A Thesis

Submitted to the Faculty

of

Purdue University

by

Mukta V. Kulkarni

In Partial Fulfillment of the

Requirements for the Degree

of

Master of Science in Mechanical Engineering

December 2016

Purdue University

West Lafayette, Indiana

To,

Aai and Baba,

For all the support through my years of learning and growing.

ACKNOWLEDGMENTS

I would like to express my sincere gratitude towards my adviser, Dr. Peter Meckl, for granting me with the opportunity to work under his supervision and for teaching me various aspects involved in research. I am indeed thankful for Dr. Meckl's continuous support during my years at Purdue and for his patience, motivation and immense knowledge. A big thank you to my committee members, Dr. Patricia Davies and Dr. Greg Shaver for serving on my committee.

I thank Rick Reisinger, David Carey and Donald Benson at the Fuel Systems Specific Controls Team at Cummins Inc., for their timely support, useful inputs during the course of this research and for sponsoring this research project. I would also like to express my gratitude towards them for giving me an opportunity to intern at Cummins Fuel Systems. I am thankful to Wei Ning from Cummins Inc., for his guidance with the software aspects involved in this project.

I am deeply indebted to Shambhavi Balasubramanian for mentoring me during my first year as a researcher on this project. I would like to thank Saurabh Saboo for his invaluable assistance during my research.

I wish to express my sincere thanks to Ryan Tooley from Gamma Technologies for his reliable assistance during the course of this research. I am grateful to all my colleagues at Herrick Laboratories for making this journey an enjoyable one with their constant support in times of need. A special thanks to Donna Cackley and Cindy Cory of Herrick Laboratories for always taking care of the logistics involved during presentation meetings. I thank Cathy Elwell and Julayne Moser of Mechanical Engineering for their advice in times of need.

A special thanks to all my friends at Purdue for their unwavering support and for being like a family to me away from home. My deepest thanks to my parents for their constant words of encouragement, support and for always being there for me.

TABLE OF CONTENTS

Page

LIST OF TABLES

LIST OF FIGURES

Figure Page

SYMBOLS

m	mass
P	pressure
T	temperature
V	volume
β	bulk modulus
ρ	density

ABBREVIATIONS

B100	100% Biodiesel Fuel
CCR	Cummins Common Rail
ECM	Engine Control Module
FFT	Fast Fourier Transform
FIR	Finite Impulse Response
GT	Gamma Technologies
IIR	Infinite Impulse Response
IMV	Inlet Metering Valve
PSD	Power Spectral Density
SOI	Start of Injection
XPI	Extreme-high Pressure Injectors

ABSTRACT

Kulkarni, Mukta V. M.S.M.E., Purdue University, December 2016. Determining Fuel Type from Estimates of Bulk Modulus Using Rail Pressure Measurements. Major Professor: Peter H. Meckl, School of Mechanical Engineering.

The intention of this project is to measure fuel properties that would lead to determination whether the fuel is diesel or biodiesel. This research is focused on developing strategies to estimate the isentropic bulk modulus, which is a critical parameter for fuel characterization. Bulk modulus of fuel affects pressure rise due to pumping events differently for different fuels. With the help of sensors available on Cummins XPI fuel system, obtaining the data for pressure rise is accomplished. The pressure rise information is extracted from raw transient rail pressure data after filtering. The effects of filtering, engine speed and sampling rate have been taken into account while extracting the pressure rise estimates. The results obtained from test data have been applied on data from simulation models and from a test rig, which include high frequency oscillations due to sensor noise and rail dynamics. The bulk modulus estimation technique in this research is able to estimate the bulk modulus value for diesel fuel, with errors in the range of 0.71% to 2.89%, depending on pressure. The difference in values for bulk modulus of diesel and biodiesel is 7%, which is not high enough to accommodate the uncertainties produced from bulk modulus estimation calculations. The value of ΔV used for bulk modulus changes with changing pressure and depends on the compressibility of the fuel, which in turn is dependent on the bulk modulus of the fuel. A possible approach to tackle this problem is to develop equations that use tangent and secant bulk modulus and their inter-relationship to determine ΔV and bulk modulus simultaneously from data collected at several rail pressures. Apart from this, several recommendations have been made in order to reduce the uncertainty in the results for pressure rise as well as bulk modulus estimation.

1. INTRODUCTION AND LITERATURE REVIEW

1.1 Introduction

In the drive to meet the challenges of fossil fuel depletion, environmental degradation and stringent emission controls, alternative fuels are gaining increased interest for transportation and other uses [1–3]. Biodiesel is one of the alternative diesel fuels derived from vegetable oil by transesterification. Transesterification is defined as, "a process by which plant oil or animal fat is chemically combined with excess alcohol in the presence of a basic or acidic catalyst to remove glycerine from the oil or fat molecular structure to make it suitable for use in a diesel engine" [4]. Owing to its better ignition quality, comparable energy content, higher density, non-toxic character, cleaner burning and compatibility with diesel engines without any hardware modifications, various researchers have concluded that biodiesel has great potential as alternative to diesel fuel [5].

According to data published by the U.S. Department of Energy, the production of biodiesel has increased from 8.58 million gallons in the year 2001 to 1240 million gallons in 2014, which highlights the increasing trend in biodiesel availability [6]. Biodiesel is primarily used to power diesel engines as it is functionally identical to petroleum diesel. The benefits of using biodiesel include reduced emissions of carbon monoxide (CO) and unburned hydrocarbons (UHC), although an increase in the emissions of oxides of nitrogen (NO_x) and PM (particulate matter) is seen. Nitrogen oxides and PM are considered the most harmful gaseous emissions from engines. However, engine researchers are investing their efforts in developing techniques to reduce these emissions through exhaust gas recirculation, selective catalytic reduction,water diesel emulsion, etc [7, 8].

Biodiesel can be blended and used in a variety of concentrations. The most common blends of biodiesel are B20, B5, B2 and B100. B20 contains 6% to 20% biodiesel blended with petroleum diesel whereas B5 consists of 5% biodiesel with 95% petroleum diesel and B2 has 2% biodiesel blended with petroleum diesel. Pure biodiesel, B100, is rarely used as a transportation fuel and its typical use is as a blendstock for the production of B5 and B20. Studies show that, with an increase in percentage of biodiesel, there is an increase in fuel consumption and NO_x emissions and a decrease in the peak of heat release rate (PHRR), which is disadvantageous, as this leads to an increase in the quantity of fuel injected to reach required heat release and therefore, reduces the fuel economy [9].

1.2 Diesel vs. Biodiesel

Diesel fuels are mainly composed of paraffinic and olefinic compounds of varying chain length, whereas the main constituents of biodiesel are saturated and unsaturated methyl esters of chain lengths in the range of C14 to C24 [10]. Production of petroleum diesel is done by fractional distillation of crude oil, which results in a mixture of carbon chain lengths in the range of C8 to C21 [11].

Research shows that UHC emissions decrease to 78% and CO emissions decrease to 81% with biodiesel blends as compared to diesel. Biodiesel typically contains 10% additional oxygen than diesel, which ensures complete combustion of remaining fuel. The brake power for biodiesel has lower values, while BSFC (brake specific fuel consumption) has higher values than those for diesel. However, NO_x emissions are seen to increase by 15% with biodiesel as compared to diesel at full load conditions [5]. Biodiesel has an earlier start of combustion (SOC) than diesel, which is a result of advanced injection timing from higher density and bulk modulus and lower ignition delay of biodiesel due to a higher cetane number [9].

Lubricity is a factor of a fuel that prevents wear on contacting metal surfaces in critical engine parts such as fuel injection pump or fuel injector. High wear and scar-

ring may be caused by low lubricity whereas reduced wear and enhanced component life is provided with a high-lubricity fuel. Biodiesel blends show up to a 65% improved lubricity compared to diesel fuels.

Fuel injection characteristics are affected by fuel system parameters and fuel properties such as bulk modulus, speed of sound, density and viscosity [12]. The differences in behavior of diesel and biodiesel due to the differences in their characteristics are discussed in the literature review that follows.

1.3 Objectives and Motivation

Devising strategies for fuel type determination is an exploratory step towards designing adaptive injection control. Parameters such as fueling quantity, on-time of injectors and timing of injections are affected by the type of fuel. These parameters can be controlled to deliver better performance and higher efficiency of the fuel system if the type of fuel is known.

This research covers the strategy to determine the fuel type by estimating the bulk modulus of the fuels under consideration. The fuels under consideration are diesel D2 and biodiesel B100. The fuel system under consideration consists of Cummins Scania XPI injectors, which are high-pressure and solenoid-actuated injectors. The algorithm developed on test data from GT-simulations has been tested on data obtained from a Cummins test rig. This research, in particular, focuses on the transient rail pressure data to estimate the bulk modulus of the fuel.

1.4 Literature Review

The various sources of biodiesel fuel and engine technologies make it complicated to conclude the impact of biodiesel combustion on engine behavior, especially in transient state operation. As diesel (D2) and biodiesel (B100) are obtained from different sources and by different methods, their fuel properties differ from each other as well. This leads to a difference in their injection, combustion and emission characteristics.

As a result, a diesel engine does not operate with the same characteristics with B100 as the fuel as it will operate with D2 as the fuel [13]. The main focus of the bulk modulus estimation algorithm, as will be seen in chapters 3 and 4, is on the pressure rise due to pumping. This section gives a brief overview of findings of other researchers on bulk modulus and their usefulness in determining the bulk modulus.

The fundamental principle of bulk modulus can be explained as a reduction in liquid volume under a sufficiently high pressure. Knowing the change in volume due to change in pressure, the adiabatic or isentropic bulk modulus for a fuel can be calculated by [14]:

$$\beta_{isentropic} = -V_s\left(\frac{\delta P}{\delta V}\right)_{isentropic} \tag{1.1}$$

In case of an isothermal system, the isothermal bulk modulus is calculated by:

$$\beta_{isothermal} = -V_s\left(\frac{\delta P}{\delta V}\right)_{isothermal} \tag{1.2}$$

Isothermal and isentropic bulk modulus are related to each other by specific heat ratio, γ as follows [15]:

$$\beta_{isentropic} = \gamma \times \beta_{isothermal} \tag{1.3}$$

To predict the behavior of fuel injection systems, it is necessary to know the pressure dependence on bulk modulus for various fuels. A series of measurements taken by Payri, et al. showed that the dependency of bulk modulus on "pressure is almost linear and increases with pressure." Some researchers have suggested that "the lower bulk modulus of fuels at lower pressures is because of the existence of free space between the loosely packed molecules. When the pressure increases, the bulk modulus also increases" due to compression of molecules [16]. More details can be found in [17].

Figure 1.1 illustrates the bulk modulus at two sample temperature values, for sample fuels that include D2, Arctic (Winter) fuel and Rape Methyl Ester (biodiesel)

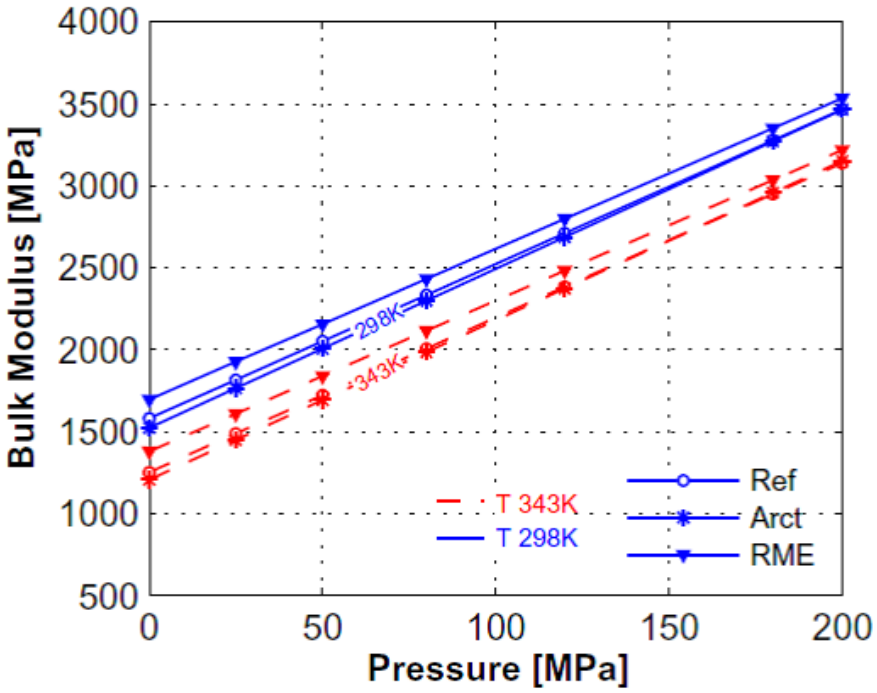

Figure 1.1. Isothermal bulk modulus curves for diesel Fuel, Arctic (Winter) Fuel and Rape Methyl Ester (biodiesel) [16].

fuel. Figure 1.2 shows the variation of bulk modulus values at constant pressures, for the three fuels. The data obtained from the measurements taken by Payri, et al. is fitted to a polynomial expression, to give a dependence of bulk modulus on temperature and pressure [16] as follows:

$$\beta = k_1 + k_2(T - T_o) + k_3(P - P_o) \tag{1.4}$$

Bulk modulus values for biodiesel are seen to be higher than those for the remaining fuels. Researchers have reported that having a lower compressibility, and thus, a higher bulk modulus, results in a faster pressure rise produced by the pump [5]. There is a 7% increase in the bulk modulus values for biodiesel, when compared to diesel fuel. This implies that, for bulk modulus estimation for two fuels, the strategy

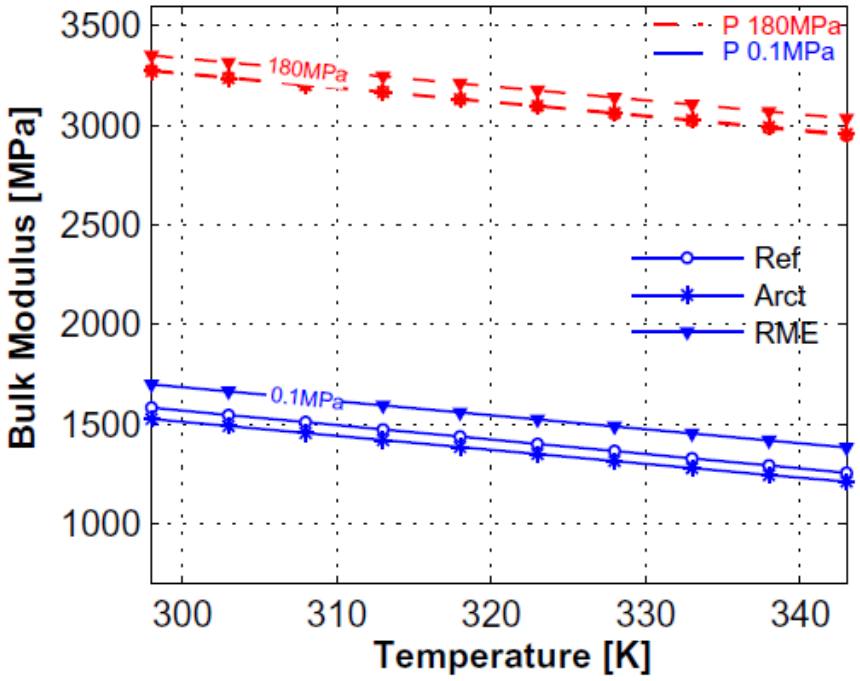

Figure 1.2. Isobaric bulk modulus curves for diesel fuel, Arctic (Winter) Fuel and Rape Methyl Ester (biodiesel) [16].

developed should be able to estimate values that have an uncertainty much lower than 7%, in order to accurately determine the fuel type.

In one approach to determine the bulk modulus of a fuel using the high-pressure pump, shown by Sakai, et al. in U.S. Pat. No. 7,007,662 [1], an Electronic Control Module (ECM) learns the bulk modulus of fuel by utilizing the fuel pressure before and after actuation of the high-pressure pump. In this method, the ECM calculates the pressure difference while also calculating the amount of fluid discharged from the high-pressure pump. However, Pursifull, et al. in U.S. Pat. No. 9,243,598 [2] pointed out potential issues with the approach developed by Sakai, et al. First, it may be difficult to obtain a usable pressure signal from the pressure sensor while the high-pressure pump and fuel injectors are actively maintaining fuel flow, which may cause pressure waves that affect pressure sensor readings. Furthermore, utilizing a

measure of actual fuel volume pumped from the high-pressure pump, or injected into the engine from the injectors, may be difficult and yield uncertain results.

Pursifull, et al. suggested a method to address the issues in the approach by Sakai, et al. The method comprises of adjusting the duty cycle of the high-pressure pump to measure bulk modulus of a fuel "based on a zero flow function for the high-pressure pump, the fuel being pumped through the high-pressure pump and the zero flow function based on a change in pump duty cycle relative to a resulting change in fuel rail pressure." It was recognized by the researchers of this patent that the slope of the flow function is directly proportional to the fuel's bulk modulus [2]. This approach enables continuous and reliable calculation of bulk modulus of the fuel on-board the vehicle.

Balasubramanian [12] developed a strategy for finding the isentropic bulk modulus of a fuel by filtering the steady-state rail pressure signal and calculating the pressure rise. The performance of the technique was statistically analyzed for D2 and B100 fuels to determine the ability of the algorithm to correctly determine the fuel type. However, it was concluded that issues such as variation in the pumping volume with respect to pressure lead to overlap of the diesel and biodiesel estimates and causes ambiguity in fuel type determination.

The technique developed by Balasubramanian has been further improved upon in this thesis, by refining filtering techniques, developing better pressure rise estimates and understanding the physics behind variability of fuel volume pumped with respect to pressure. Transient rail pressure data has been considered to conduct all the tests.

1.5 Thesis Overview

The contents of this thesis are spread across five chapters. The first chapter, i.e., the current chapter, discusses the problem statement, the motivation behind it and the study of differences in characteristics of diesel and biodiesel in the form of a brief literature review. Chapter 2 involves a description of the simulation models

in GT-Power software, based on the Cummins Scania XPI fuel system, as well as simulation models developed to test details concerning the physics of the proposed bulk modulation estimation strategy. Chapter 3 gives a detailed description of the steps in bulk modulus estimation. Chapter 4 describes analysis of filter effects on the rail pressure data and results from applying the bulk modulus algorithm on simulation and test rig data. Chapter 5 highlights the conclusion, summarizes the thesis, and discusses recommendations and future work.

2. SIMULATION MODELS

The results obtained from the test cases to be described in chapter 4 need to be tested with the help of data obtained from models in GT-Suite. The simulation models are helpful in obtaining rail pressure data at various rail pressures and pumping frequency conditions. GT-Suite is a simulation tool from Gamma Technologies that is aimed at automotive engineering applications and helps the user with detailed system or sub-system analyses. GT-Suite consists of two main applications :

1. GT-ISE (Integrated Simulation Environment): The models are built and simulation settings are declared in this application. The Library consists of various compounds and templates that can be used as necessary while modeling.

2. GT-POST: Results of the simulation are viewed in this application. The parameters of the model to be analyzed that are set in GT-ISE can be viewed graphically as well as numerically in GT-POST.

2.1 Need for a Simulation Model

The test cases to be described in chapter 4 demonstrate the effect of filtering on an idealized case of transient rail pressure. However, as will be explained in later chapters, the test data is created to imitate the transient data waveform but without including any pressure oscillations or noisy measurements. To verify the results obtained from the test cases, it is necessary to have a simulation model that gives rail pressure data that includes the oscillations in the system. The simulation data is closer to the actual real-time rail pressure data on which the algorithm would be applied. Simulation models give the flexibility to rapidly collect data over multiple rail pressures and pumping interval specifications.

2.2 Fuel Modeling in GT-ISE

In addition to simulating the models with the fuels present in the GT-Suite library, there is a provision to custom-define fuel objects in GT-ISE. This is necessary to get rail pressure data for multiple fuels. The diesel fuel, D2, is already defined in the GT-Suite library. To examine the variation in bulk modulus estimates between diesel and bio-diesel, a bio-diesel fuel object has been custom-defined by giving the density, bulk modulus, and sonic speed values as functions of temperature and pressure. All the tests in this thesis have been performed with D2 as the fuel, unless otherwise stated.

2.3 GT Models

The data of prime importance to estimate the bulk modulus of a fuel is the pressure rise due to pumping. The fuel system model consists of the fuel injectors, pump and the common rail. This section describes the different simulation models set up in GT-Suite to build the Cummins Fuel System.

2.3.1 Pump Model

The Cummins Fuel System consists of a two-chamber pump as shown in Figure 2.1. The pump is a positive-displacement pump that operates in high-pressure conditions. The components of the high-pressure pump are described below:

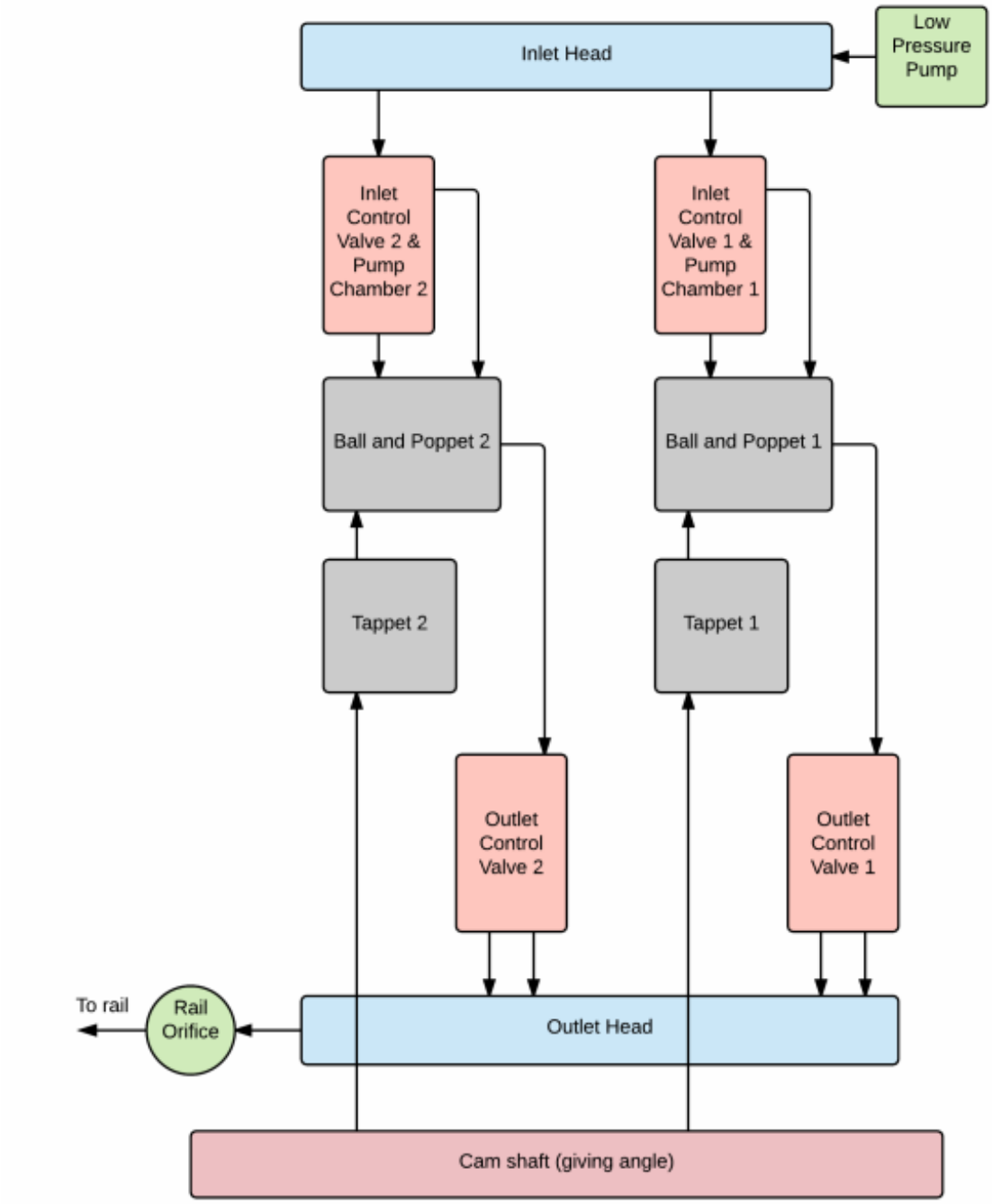

Figure 2.1. Block diagram of pump model [12].

1. Low-Pressure Pump - The low-pressure pump performs two main functions that include delivering fuel to the high-pressure side and cleaning the fuel. The

pump output can be changed by modifying the pressure in the low-pressure inlet volume. In an actual engine, the pump consists of a pressure regulator valve or the inlet metering valve (IMV) to avoid high pressures caused by high pump rotation during high engine speed. This element has not been included in our model.

2. Inlet Head, Inlet Control Valve and Pump Chamber - While the pump chamber is filling up with fuel, the inlet valves are opened and the outlet valves are closed. The plunger facilitates the displacement of the pump chamber, which enables calculation of change in volume due to pumping.

3. Outlet Control Valve and Outlet Head - The fuel from the pump is pumped into the rail through the rail orifice. The outlet valves open in order to discharge the fuel through the rail orifice with the inlet valves closed.

4. Rail Orifice - The pumping of the fluid is controlled by the opening and closing of the Outlet Control Valves. The outlet end of the rail orifice can be merged to the rail.

Depending on the requirements for pumping intervals, the ratio between pump RPM and engine RPM can be set equal to or greater than 1.0. For analysis in transient applications, pumping intervals of 90, 180 and 360 crank angle degrees have been considered for the analysis of accurate pressure rise estimation in order to get the correct bulk modulus estimate for the fuel. This pumping interval variation can be achieved by changing the cam displacement profile that actuates the plunger in the pump model, which affects the pumping interval.

The simulation consists of a low-pressure source. This pressure source can be constant or variable. In the simulations executed, the pressure has been kept constant, which may not be the case in real-time engine operations.

One advantage of simulation with the GT model is the ability to observe the pressures and fluid volumes in the pipe elements, which are not readily available in

an actual pump. These values of parameters of interest can be viewed in outputs as pressures in Pump Chambers, Inlet Head and Outlet Head. The total volume of fuel that is pumped into the rail is the sum of the fluid volumes from both Outlet Control Valves.

2.3.2 Pump Cutout Model

The Cummins Fuel System consists of the Cummins Common Rail, which is a direct fuel injection system that uses six Cummins XPI injectors. The range of pressures on which the Cummins Common Rail operates is about 500 bar to 2600 bar. The specification "XPI" stands for Xtreme High Pressure Injection. The XPI injectors are solenoid-actuated injectors that can fire up to 2 pulses per cylinder event (limited primarily by the existing software). The primary applications of these fuel systems are in heavy-duty and mid-range applications.

The main components of the pump cutout model are the injectors and the rail connected to the injectors. The name "pump cutout" comes from the fact that this fuel system model does not include the pump. To regulate the fueling of the injectors to 100 mg, which has been set in the simulation, there is a pressure sensor in the rail that communicates the rail pressure to the controller for injectors. Based on the rail pressure, the on-time of the injectors is controlled to maintain the fueling of the injectors. Figure 2.2 shows the block diagram of the pump cutout model.

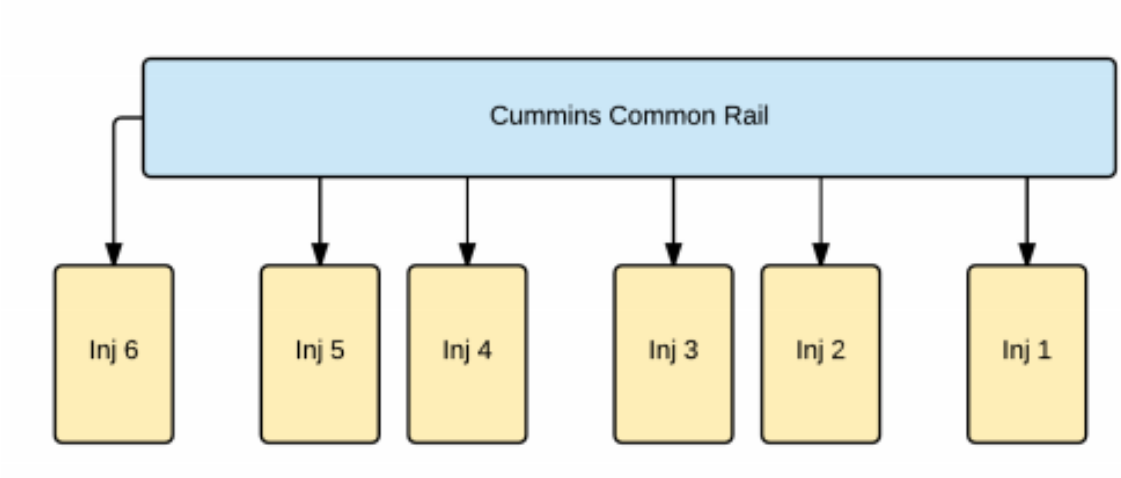

Figure 2.2. Block diagram of pump cutout model with Common Rail and injectors [12].

The injections occur every 120°, which means that every injector fires once during the course of 720° revolution of the crank-shaft. The injection order is decided by the order in which the cylinders reach the combustion stroke. Table 2.1 shows the firing order of the injectors.

Table 2.1. Injector order for Cummins Common Rail.

Crank Angle	Injector Firing
0	Injector 1
120	Injector 5
240	Injector 3
360	Injector 6
480	Injector 2
600	Injector 4

Due to the injection of fuel, there is a pressure drop seen in the rail pressure. For a starting rail pressure of 2500 bar and engine speed of 1000 RPM, there is

approximately a 40-bar pressure drop in the rail for every injection event. This results in a downward "staircase" waveform as shown in Figure 2.3. The corresponding injection events are shown in Figure 2.4. It can be seen that the mass flow rate at every injection decreases with every injection. The change in pressure causes a change in flow rate. As the fueling is set to be constant at 100 mg, the on-time changes with a change in the mass flow rate of the injection.

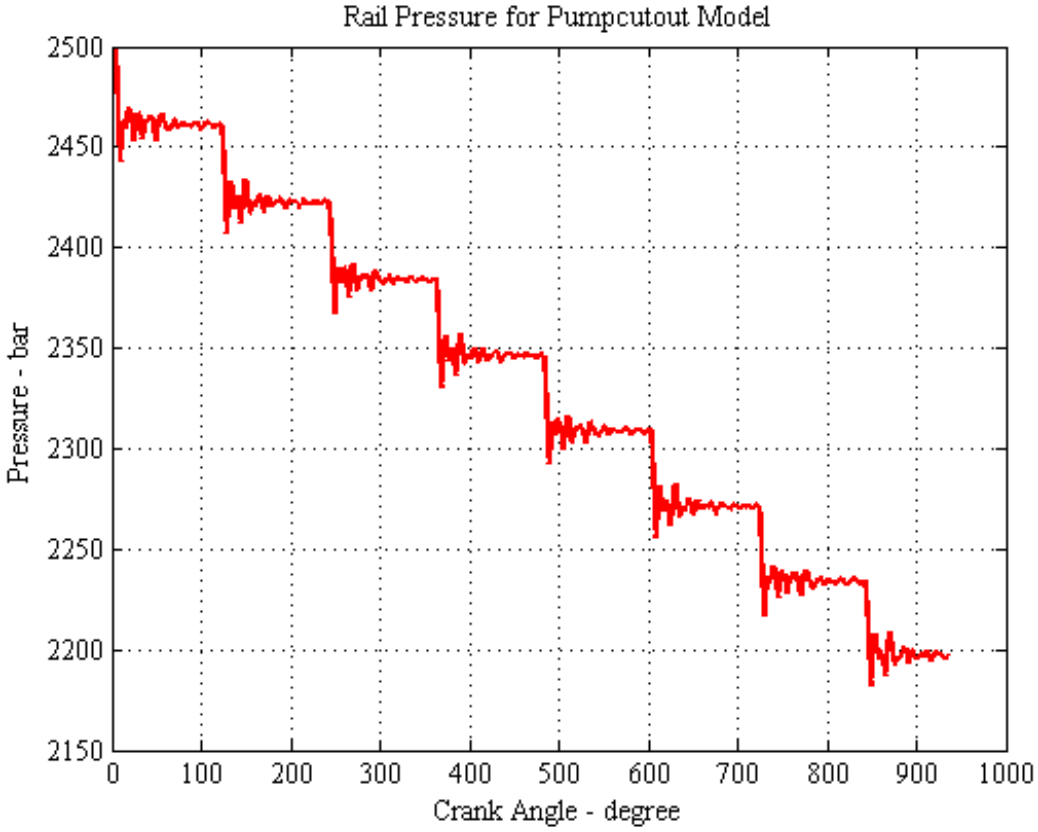

Figure 2.3. Rail Pressure for pump cutout model with starting rail pressure of 2500 bar at 1000 RPM.

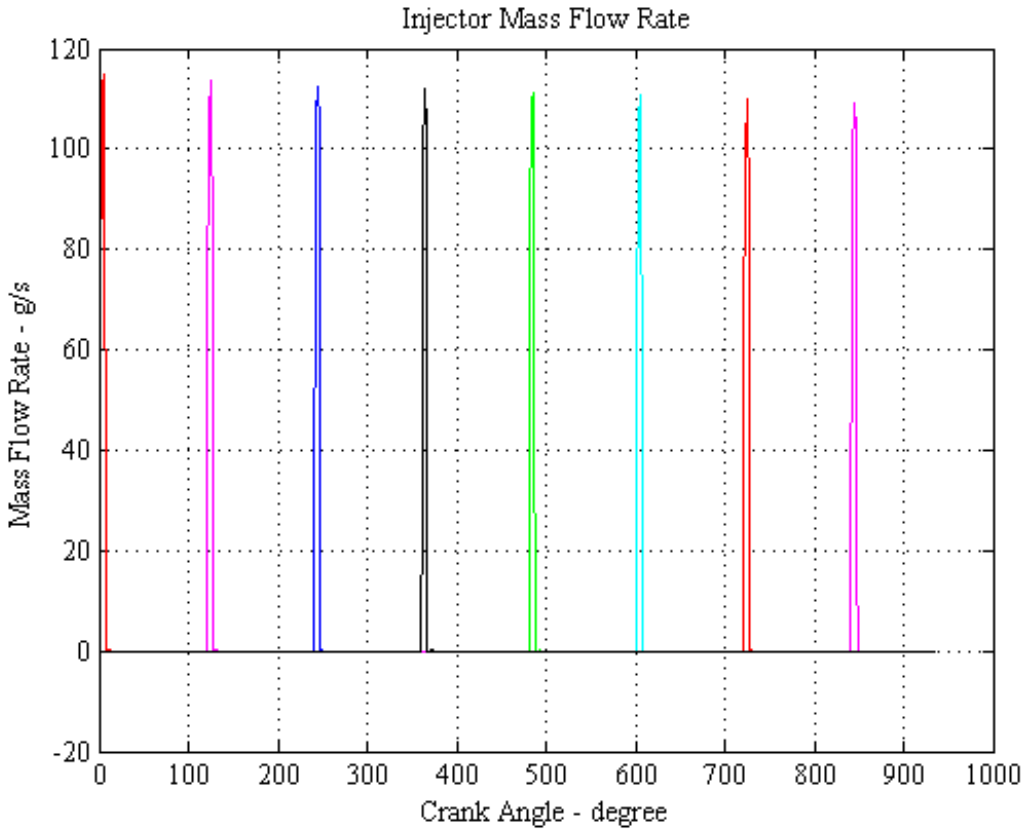

Figure 2.4. Injection events corresponding to pressure drop in rail pressure.

2.3.3 Combined Model

The pump model along with the pump cutout model can be combined to form the Cummins Common Rail XPI Fuel System in GT-Suite. The fuel from the pump is passed on to the rail through the high-pressure pump-to-rail tubing through the rail-in orifice from the outlet check valve (OCV) of the pump. As the pump consists of two elements each, there are two connections going from the pump side to the rail. The three main components of this combined model are the injection system, high-pressure pump and the rail. While the injection system, the high-pressure pump and rail are represented with elaborate components in the GT model, the low-pressure

system is just represented using a low-pressure source. Figure 2.5 shows the schematic of the Cummins Common Rail XPI fuel system.

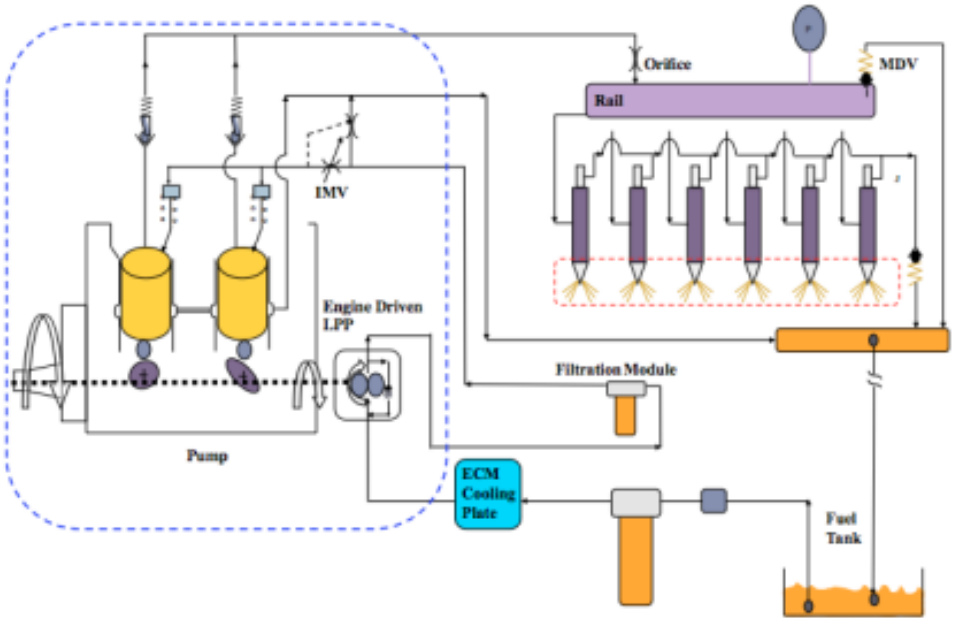

Figure 2.5. Schematic of Cummins Common Rail XPI fuel system [18].

The pressure in the rail is to be maintained between a pressure range of 500 bar-2600 bar. In order for this to happen, there is a mechanical dump valve (MDV) present on the rail that dumps excess pressure out from the rail if the pressure goes higher than the operating pressure range of the fuel system. However, this dump valve has not been included in the GT model. To meter the amount of fuel that is taken into the pump, there is an inlet metering valve (IMV) present between the low-pressure pump and the high-pressure pump. The IMV can be fully or partially open, giving either a full pumping event (maximum fuel delivery) or a partial pumping event that does not provide all the fueling from a full pumping event. The drawback of the fuel system we are working with is that there is no way of knowing the amount of opening of the IMV. The GT-model does not include the IMV, so all the pumping events in

the simulation can be assumed to be "full" pumping events. Figure 2.6 shows a block diagram of the combined model.

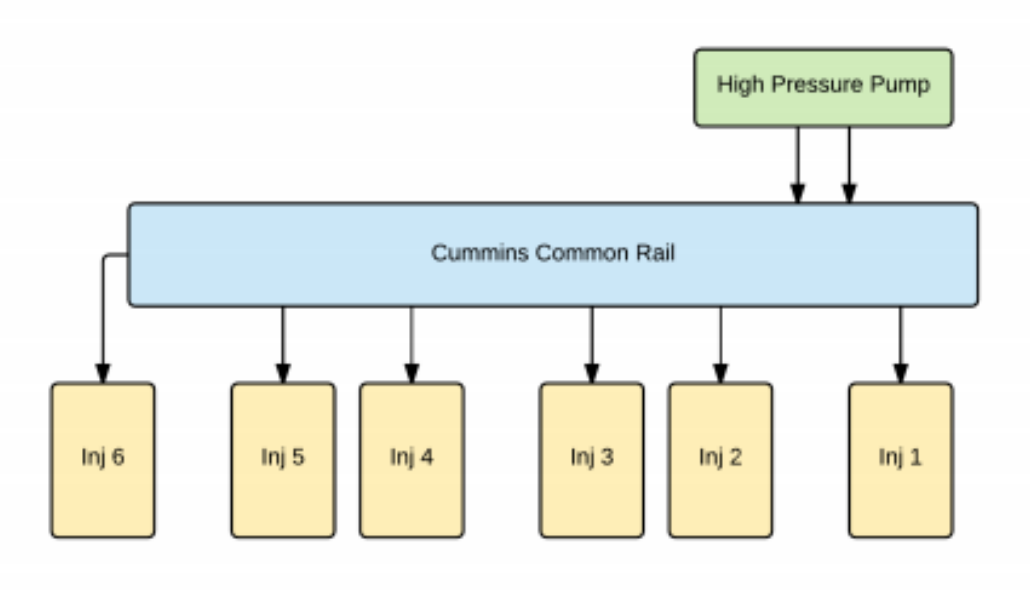

Figure 2.6. Block diagram of Cummins XPI fuel system [12].

- **Combined Model Without Injections**: The timing of the pumping events can be controlled by fueling requirements. The transient rail pressure analysis for bulk modulus estimation is best done when there are no pressure drops due to injections involved. Rail pressure data with no influence from injections gives clean data that involves only pressure rise from pumping events. This makes the pressure rise estimation algorithm of bulk modulus simpler as the step of identifying clean pumping events can be eliminated.

  In order to eliminate the injection events in the combined model, a few modifications have made. These include:

  1. The injectors are removed completely and substituted by a closed volume that is equal to the volume of all the injectors and the volume of all the tubing from the rail to injectors. This volume is added to the rail volume.

This ensures that the volume of the system is maintained without any pressure drop due to injections.

2. The outlets from the two pump elements are given to the rail-and-injector combined volume by a single pipe through the high-pressure pump-to-rail chambers.

Figure 2.7 shows the transient rail pressure waveform for a starting rail pressure of 950 bar at 1000 RPM with 180° of crank angle spacing between two pumping intervals. Figure 2.8 shows the corresponding pumping events for each of the pressure rises in Figure 2.7.

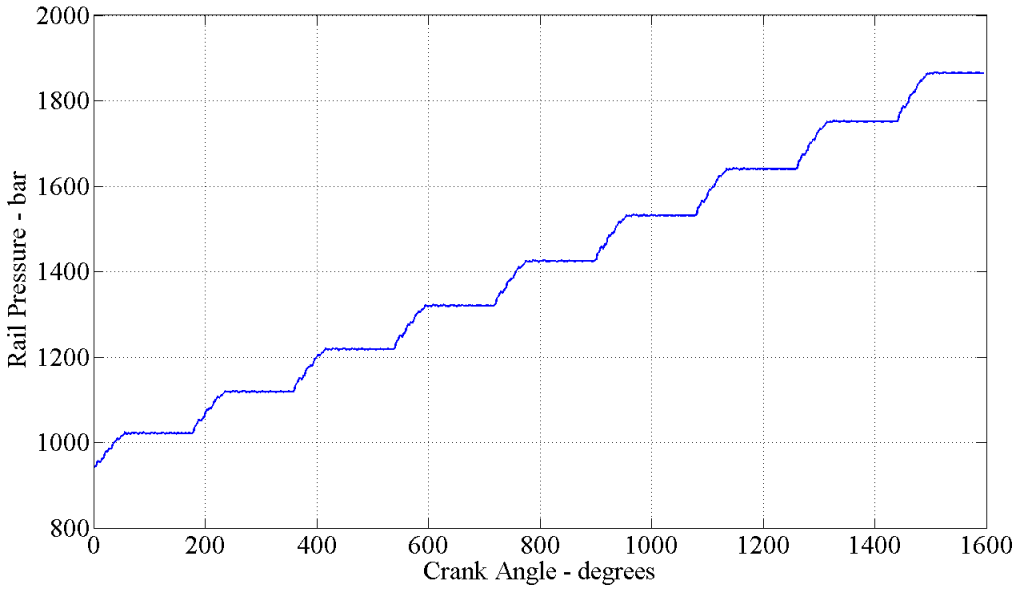

Figure 2.7. Rail pressure - no injections, pumping only with starting rail pressure of 950 bar at 1000 RPM.

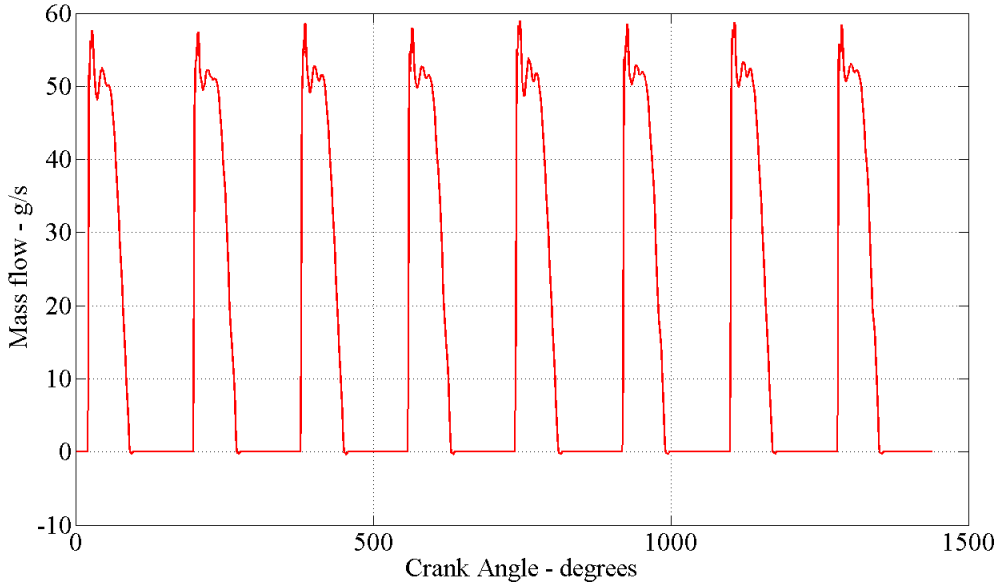

Figure 2.8. Pumping events spaced 180° apart.

- **Controlling Pumping Interval**: The GT pump model obtained from Cummins is set to pump every 90° of crank-shaft revolution. However, analysis of the best pumping interval specification for an accurate pressure rise estimation requires data with different pumping intervals to be tested. The cases of pumping interval studied here are 180° and 360° of crank angle revolution. This requires further modifications to be made in the combined model without injections.

  The pump model consists of two pumping elements that pump alternately at 90° interval. In actuality, each of the pump elements is pumping every 180°, but it appears that there is pumping every 90° as they are 90° out of phase with respect to each other and pump alternately. To have 180°-spaced pumping events, the second pump element is simply shut off. This makes only the first element pump, giving us pumping every 180° revolution of the crank-shaft.

  The cam profile consists of two lobes that represent two pumping events for the same pump element every 360° revolution of the crank-shaft. With one pump element shut off and for the other one to pump once every 360°,

the second lobe of the cam profile is made zero. This means that the piston operating inside the pump gets a maximum displacement only once every 360°. This modification in the cam-profile ensures that pumping happens only once every 360° of the crank-shaft revolution.

While making these modifications, all the tubing from the second pump-element to that rail was kept intact. This was done to be consistent with the actual hardware modification that was done while obtaining data from Cummins test rig. Retaining the original tubing from the second pump-element ensures that the overall volume of the system is intact.

Apart from the simulation models described in this chapter, other models have been created to test the underlying physics of the concepts used in the bulk modulus estimation. These models, and the results obtained from them, will be described in the relevant sections.

3. BULK MODULUS ESTIMATION - ALGORITHM

This thesis is primarily focused on fuel type determination using the bulk modulus computed from transient rail pressure data. The strategy and the steps involved in the determination of the bulk modulus are outlined in this chapter. The isentropic or adiabatic bulk modulus is given by Equation (3.1):

$$\beta_{isentropic} = -V_s \frac{\partial P}{\partial V} \tag{3.1}$$

It is assumed that the pressure and volume changes occur fast enough so that no heat transfer to surroundings can be assumed. The bulk modulus can be estimated once the two quantities, pressure rise due to pumping, ΔP, and the change in the volume of the pumping chamber due to a single pumping event, ΔV, are estimated. The following sections discuss the methods to obtain the pressure rise from the rail pressure rise signal.

3.1 Bulk Modulus Formula Analysis

Before using the formula for bulk modulus defined in Equation (3.1), it is important to understand the physics behind the bulk modulus calculation and the validation of the formula.

3.1.1 Validation of Formula

The formula can be tested with a simple piston-cylinder arrangement having a closed volume. The piston displacement causes the compression of the fuel which in effect causes change in volume, ΔV, and change in pressure, ΔP. Using these two measurements, the bulk modulus can be calculated with a known initial volume. Figure 3.1 shows a P-V diagram that describes the values of ΔP and ΔV that are considered for the calculation.

As can be seen in Figure 3.1, ΔP is the difference between P_2 and P_1 and ΔV is the difference in the volumes V_2 and V_1, where P_1, V_1 are initial pressure and volume in the pump chamber and P_2, V_2 are final pressure and volume in the pump chamber. The red lines on the plot are the slopes at the initial and final pressure and volume points. For an infinitesimal change in pressure and volume, the slopes would not change. However, since calculating ΔP and ΔV for an infinitesimal change is not possible, the δP and δV in Equation (3.1) are approximated to ΔP and ΔV. The green line on the plot shows the value for the slope which is approximated to be the value for $\frac{\Delta P}{\Delta V}$ and is used for the calculation of bulk modulus. Since the pressure rise is not instantaneous, the bulk modulus value used for verification of the formula is also not considered to be instantaneous. The bulk modulus value considered is the average of the bulk modulus values at the start of the pressure rise and the end of the pressure rise.

Taking motivation from the simple piston-cylinder arrangement, and to test the validity of the formula, a simplified model consisting of only the pump chamber and a plunger that causes compression in the pump chamber has been created. The plunger displacement is governed by the cam displacement profile that has been taken from the pump model in GT-Power provided by Cummins Fuel Systems. The model is tested for different cases of pump chamber pressure. The block diagram of this arrangement is shown in Figure 3.2.

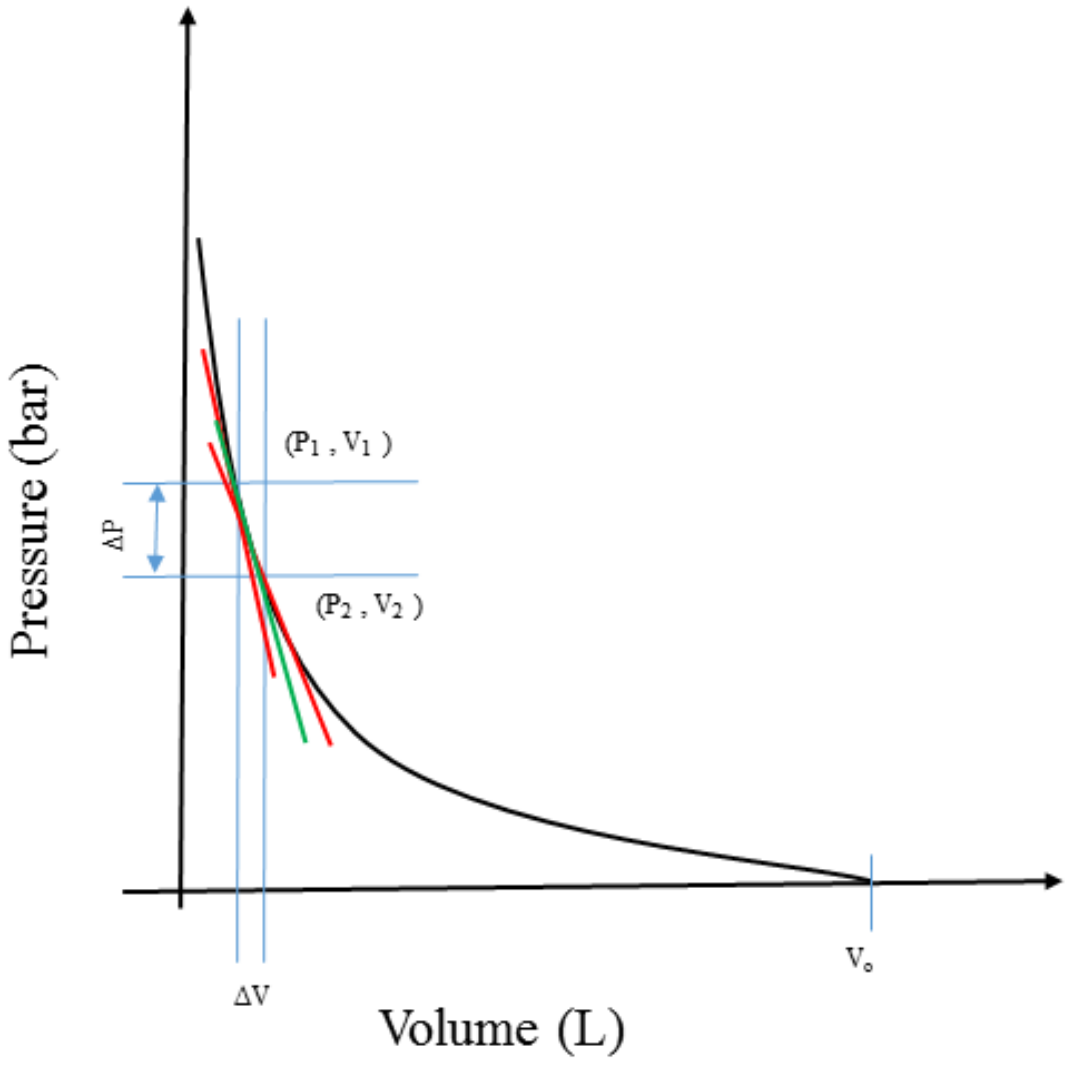

Figure 3.1. Pressure-volume plot to calculate ΔP and ΔV.

To demonstrate the calculation, consider the following case:

Initial pump chamber volume, $V = 0.007\ l$

Initial pump chamber pressure, $P = 1000$ bar

Figures 3.3, 3.4 and 3.5 demonstrate change in pressure, volume and bulk modulus, respectively.

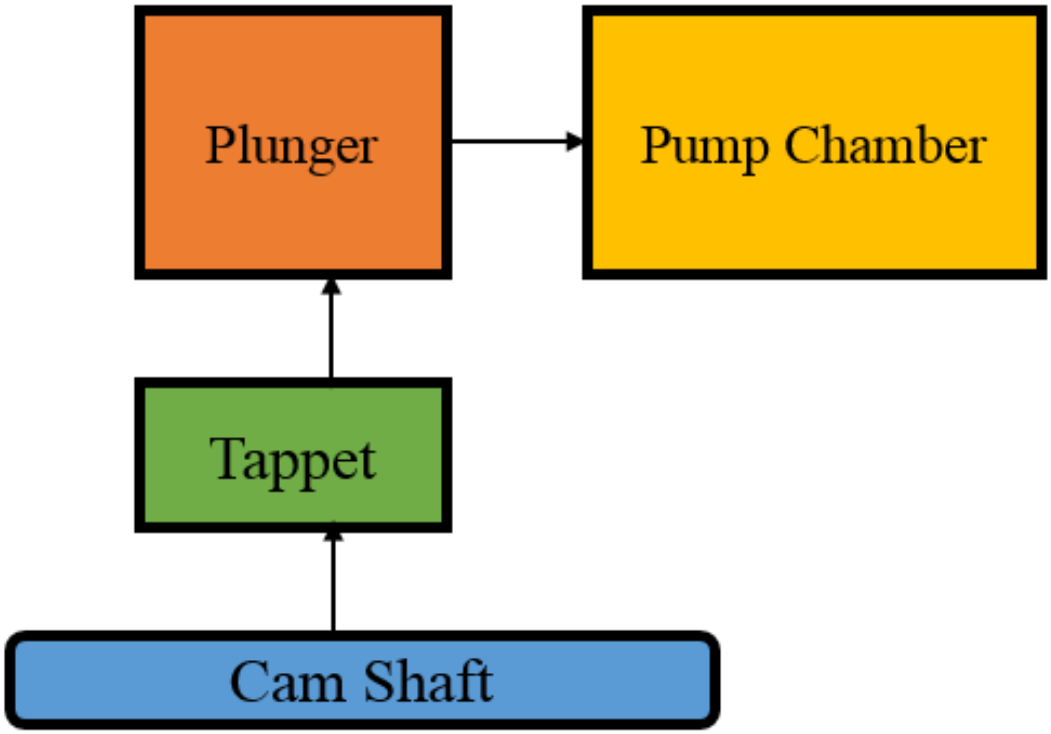

Figure 3.2. Block diagram of model used to verify bulk modulus calculation.

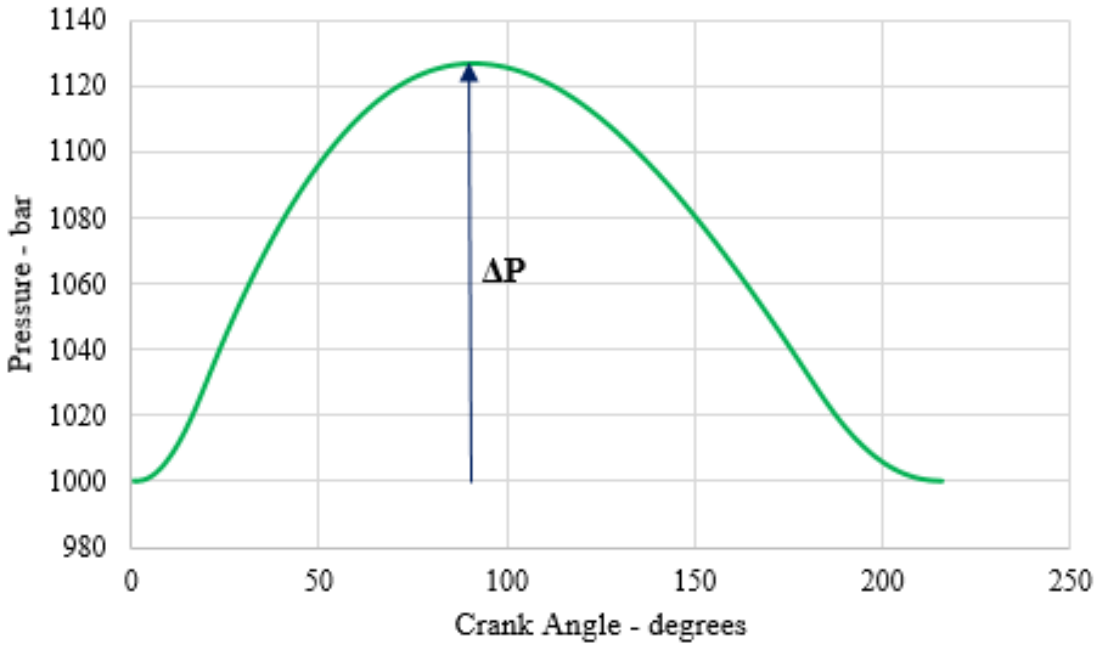

Figure 3.3. Change of pressure in the pump chamber due to displacement of plunger.

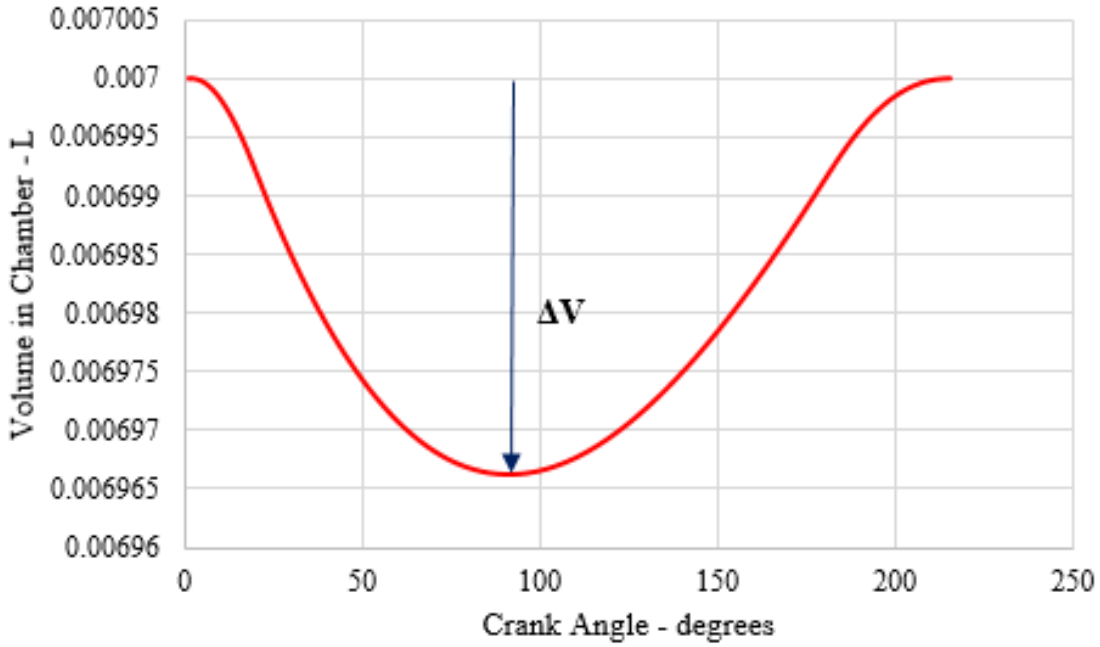

Figure 3.4. Change in volume in the pump chamber due to displacement of plunger.

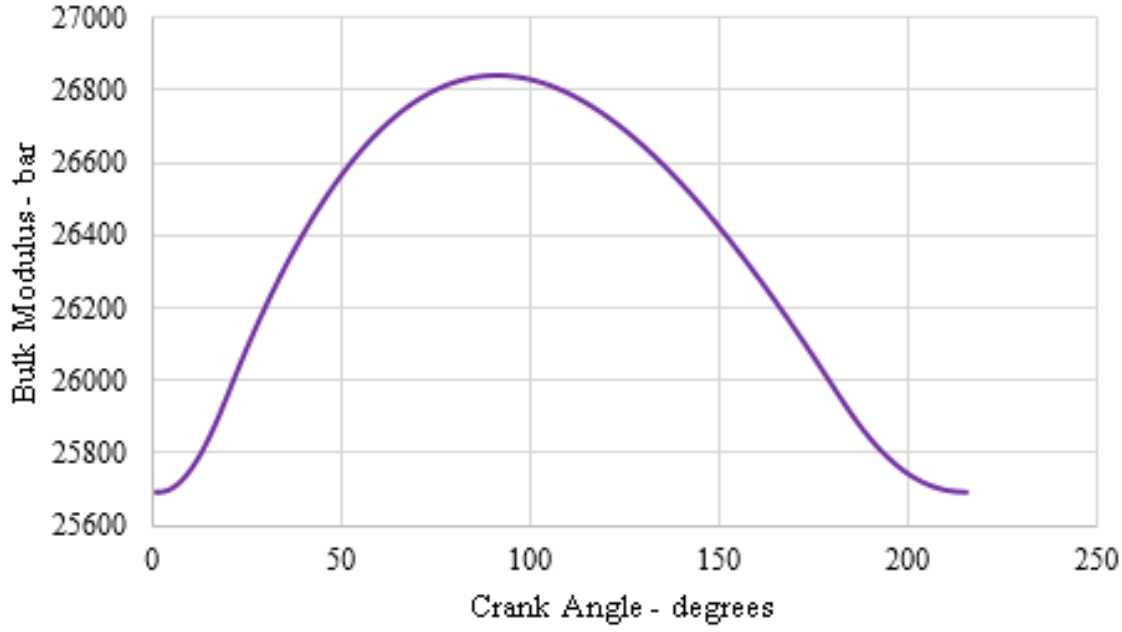

Figure 3.5. Change in bulk modulus of fuel (D2) due to displacement of plunger.

$\Delta P = 126.63$ bar

$\Delta V = -3.37 \times 10^{-5}\ L$

$\beta_{isentropic} = -V_s \frac{\Delta P}{\Delta V} = 26313.12$ bar

$\beta_{isentropic}$ from simulation = 26266.86 bar

Error between calculated value of bulk modulus and simulated value of bulk modulus = 0.1761 %.

This shows that our understanding of the bulk modulus formula is consistent with data obtained from GT-simulations. This formula has been used in all the calculations in this thesis.

The value of ΔP and change in volume ΔV are taken over an infinitesimal amount of time, which is a short amount of time for any heat transfer to take place. Therefore, there is some amount of temperature change. Hence, the process is treated as an adiabatic process and the isentropic bulk modulus is considered for all calculations instead of isothermal bulk modulus.

3.1.2 Variation in ΔV

As the displacement of the plunger is constant at all pressures, we would expect that the change in volume due to plunger displacement would be equal at all pressures, giving equal amount of fuel pumped out, at all pressures. However, the volume of fuel pumped out of the outlet valve is seen to decrease with increase in the rail pressure. The variation in volume of fluid pumped out with respect to starting rail pressure is demonstrated in Figure 3.6.

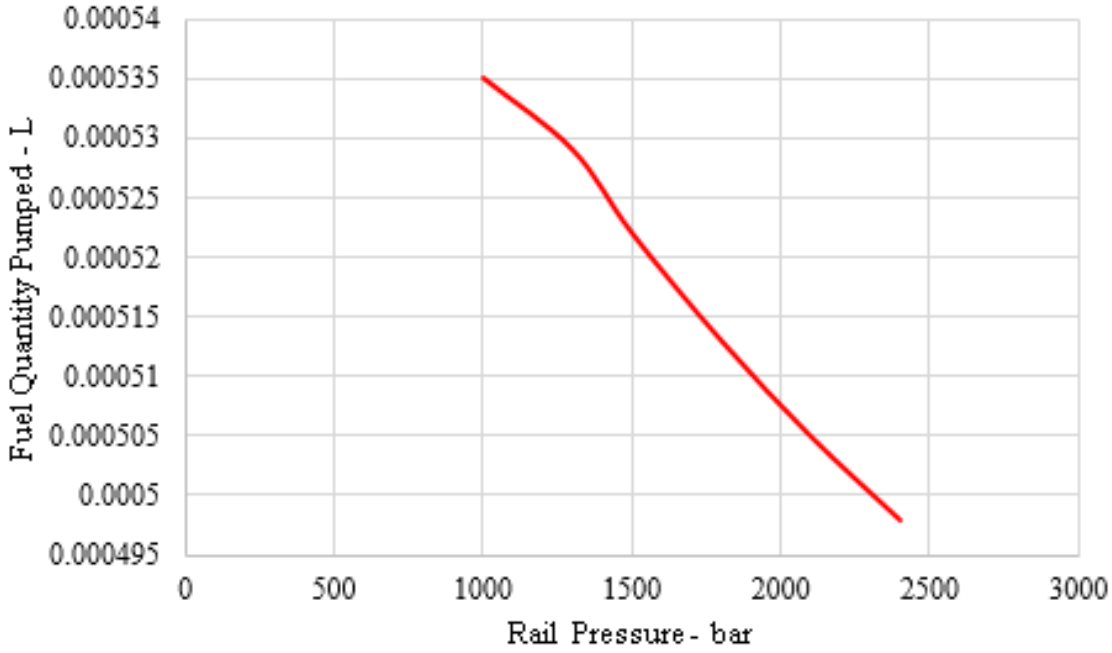

Figure 3.6. Variation in ΔV with respect to rail pressure.
(Values obtained from GT-Simulation with 180° pumping interval at 1000 RPM.)

As pressure in the rail increases, more plunger stroke is used to compress fuel against high pressure. Therefore, the effective stroke starts only once fuel has reached rail pressure. This implies that higher pressure means lower effective stroke, and hence, lower ΔV. Figure 3.7 demonstrates the start of pumping at pressures of 1000 bar and 2000 bar with respect to the volume in the pump chamber.

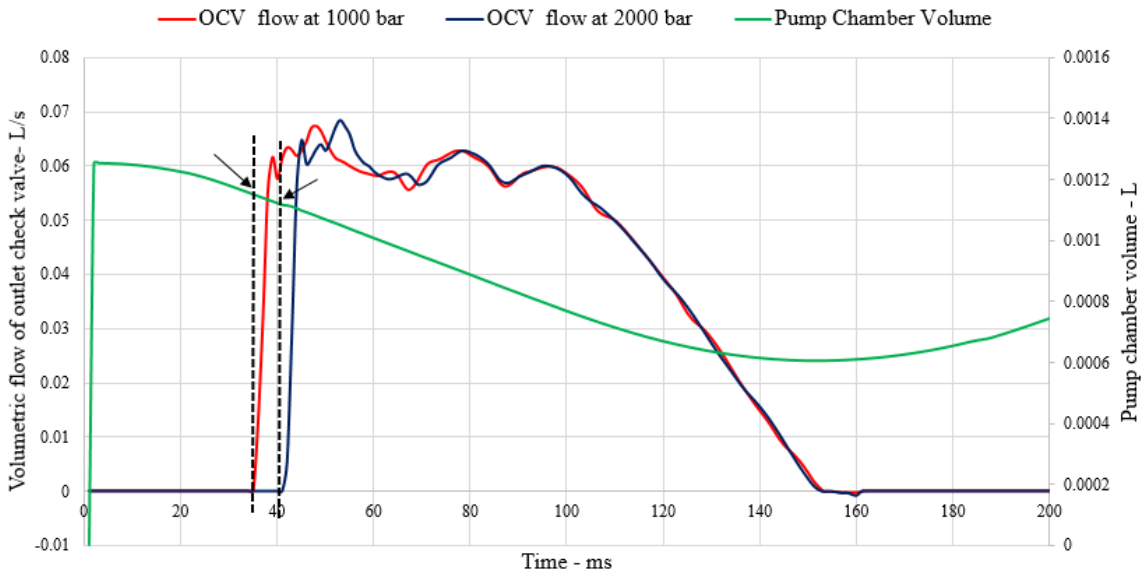

Figure 3.7. Variation in start of pumping with respect to pressure.
(Values obtained from GT-Simulation with 180° pumping interval at 1000 RPM)

Fuel flow starts later with 2000 bar rail pressure compared to 1000 bar rail pressure, and at different portions of the plunger stroke. The difference in volume of the pump chamber at the beginning of pumping for 1000 bar rail pressure and 2000 bar rail pressure is compared to the difference in fuel quantities that have been pumped out of the outlet check valve for the two different pressures. Total volumes pumped out of OCV at 2000 bar and 1000 bar rail pressure are $V_1 = 5.06 \times 10^{-4}\ L$ and $V_2 = 5.43 \times 10^{-4}\ L$, respectively, thus:

$$V_2 - V_1 = 3.65 \times 10^{-5} L \tag{3.2}$$

Volumes of the pump chamber at the beginning of stroke for 2000 bar and 1000 bar rail pressure are $V_3 = 1.116 \times 10^{-4}\ L$ and $V_4 = 1.150 \times 10^{-4}\ L$, respectively, thus:

$$V_4 - V_3 = 3.44 \times 10^{-5} L \tag{3.3}$$

Equations (3.2) and (3.3) show that the difference in pumped volume at different pressures is approximately equal to the difference in volume of the pump chamber

at the beginning of the pumping stroke for the two pressures. Above calculations confirm that the quantities of fuel pumped out vary with respect to rail pressure, according to the effective stroke of the plunger. The value of ΔV for bulk modulus calculation will, therefore, be considered according to the rail pressure at which the pumping takes place.

3.2 Overview of the Strategy

The assumptions made while designing the algorithm for bulk modulus estimation are stated below:

1. The displacement of the plunger is equal for every pumping event, but effective volume change varies with respect to pressure.
2. The pumping volume, ΔV, is a known quantity. The value for the pumped volume for various rail pressures is taken from GT-simulation.
3. There is no leakage in pumping or injection.

The Engine Control Module (ECM) performs multiple operations, which include controlling the fueling, injection timing and engine diagnostics. The rail pressure sensor continuously sends data to the ECM. This data needs to be processed in real time along with the other functions that the ECM manages to perform. It is, therefore, necessary to design an algorithm that is acceptable with respect to the computational complexity and speed of the algorithm.

Figure 3.8 demonstrates the flow of the bulk modulus estimation algorithm. The strategy consists of the steps listed below:

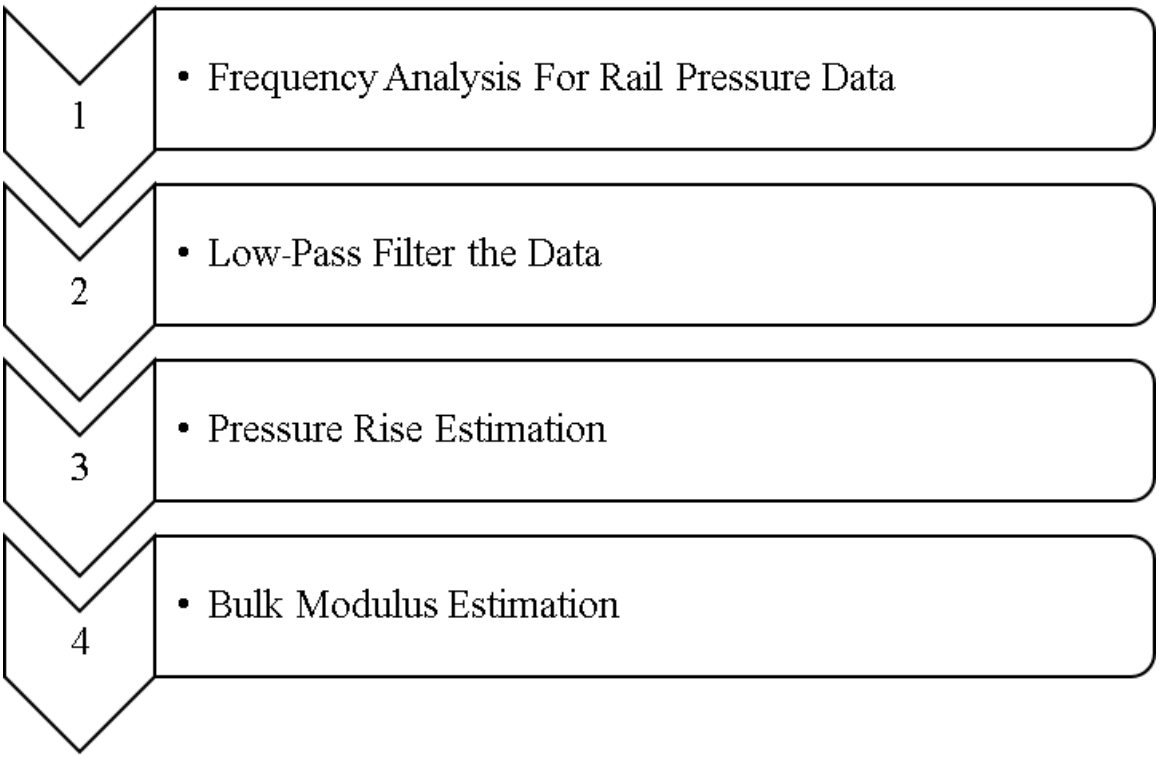

Figure 3.8. Flow of bulk modulus estimation algorithm.

1. Frequency analysis for rail pressure data - Identify the frequencies of interest and set the filter specifications such as pass band edge and stop band edge frequencies.

2. Low-pass filter the data - Reduce the noise due to sensors and other factors and oscillations due to rail dynamics in the rail pressure signal to obtain cleaner data.

3. Pressure rise estimation - Detect the clean pumping events and calculate the pressure rise due to pumping (ΔP) based on the clean events. For transient data with no injections involved, as has been considered in this thesis, detection of clean pumping events is not necessary as no injection events are involved.

4. Bulk modulus estimation - Calculate the bulk modulus from the value of ΔP obtained in step three and known values of V and ΔV.

3.3 Frequency Analysis

Frequency analysis is necessary to determine the pass band and stop band edge frequencies. The dominant frequencies in the rail pressure signal denote the pumping and the injection frequencies; depending on the pumping and injection intervals, the frequency spectrum shows peaks at these dominant frequencies. In order to make this expectation more generic, we can relate the frequencies to a known quantity, such as the engine speed (in RPM).

3.3.1 Frequency Analysis for Steady-State Rail Pressure Data

For the rail conditions under consideration, pumping occurs every 90° and there is an injection every 120° of the crank angle revolution. Therefore, for every revolution of the crank shaft, which is 360°, it can be seen that there are four pumping events and three injection events taking place in that duration. Assuming that the engine speed in RPM (E_{speed}) is known, and that one revolution of the crank corresponds to 360°, the injection frequency in Hertz is:

$$F_{inj} = E_{speed} \times \frac{3}{60} \quad \text{Hz} \tag{3.4}$$

and the pump frequency in Hertz is:

$$F_{pump} = E_{speed} \times \frac{4}{60} \quad \text{Hz} \tag{3.5}$$

An engine speed of 1000 RPM is considered for all the rail pressure data. This gives F_{inj} of 50 Hz and F_{pump} of 66 Hz. Figure 3.9 shows the frequency analysis for a starting rail pressure of 2400 bar and 1000 RPM. It can thus be verified that the dominant frequencies for the steady-state data are at 50 Hz and 66 Hz, which are the injection and pumping frequencies, respectively.

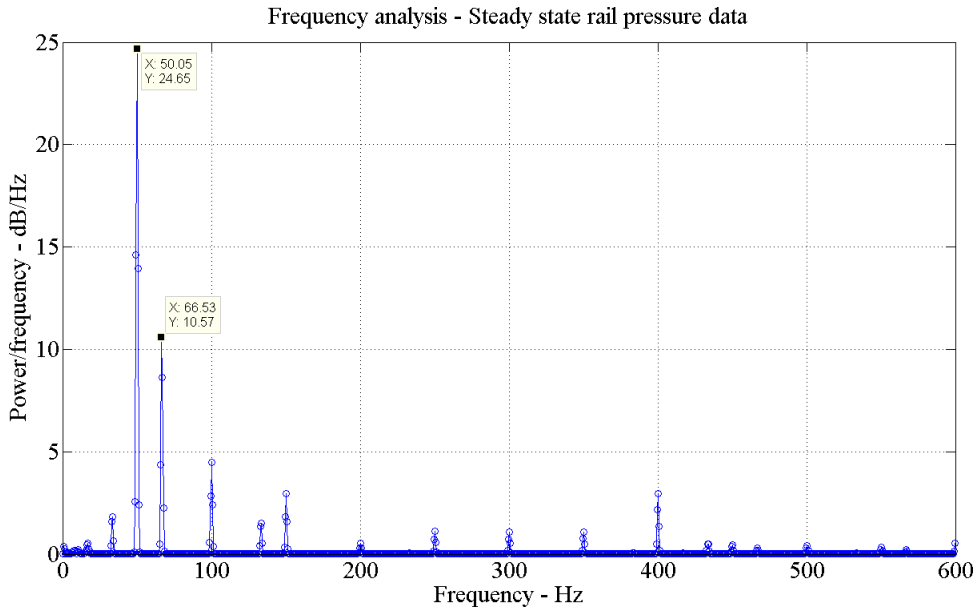

Figure 3.9. Frequency spectrum of steady-state Cummins test rig rail-pressure data for the case of 2400 bar with 90° pumping interval, 0 SOI, 1000 RPM.

Later on, pumping intervals of 180° and 360° will be considered in the absence of any injections. This changes the pumping frequency as 180° spacing will cause only two pumping events in one cycle, giving a pumping frequency of 33.33 Hz, and 360° spacing will cause only one pumping event per cycle, giving a pumping frequency of 16.67 Hz. These frequencies have been calculated for engine speed of 1000 RPM. Although we look at different pump spacings in later chapters, in this chapter, a spacing of only 90° is used.

This frequency analysis helps in determining the cut-off frequency for the filter so that the frequencies of interest are retained and frequencies of no importance can be removed.

3.3.2 Frequency Analysis for Transient Rail Pressure Data

For the frequency analyses presented below, the following process was adopted. Typically, $T_{seg} = 0.12$ seconds of data (which corresponds to $N_{seg} = 1200$ data samples) were extracted and then windowed, using a rectangular window, and a Discrete Fourier Transform (DFT) of the windowed time history was taken by using the "fft" function in MATLAB, to give X_k, $k = 0, 1, 2, N_{seg} - 1$. The one-sided magnitude spectrum was calculated: $2|X_k|/N_{seg}$. As the magnitude of the rail pressure signal is used for frequency analysis in this research, the units for magnitude spectrum used are bar/Hz, since the rail pressure signal is measured in bar and the formula for one-sided magnitude spectrum retains the original units of the signal.

In order to determine the frequency of the sine waves more accurately, the signal was zero-padded to be eighteen times longer before calculating the DFT. The Fourier Transform of a rectangular windowed sine wave results in two sinc functions centered on +/- the frequency of the sine wave. If the sampling is not synchronized with the period and thus, not a whole number of periods of the signal are transformed, which is actually the case, the true frequency will lie between the DFT points, which are k/T_{seg}. By zero-padding, the peak of the sinc function can be determined more accurately. While zero-padding does not change the true frequency resolution, it does produce a more clear picture of the underlying sinc functions, allowing for more accurate identification of the location of the peaks in the spectrum. The pumping and injection frequencies for rail pressure data, when pumping occurs every 90° and injection occurs every 120°, are 66 Hz and 50 Hz, respectively. The frequency peaks for pumping and injection frequencies are not visible in the frequency spectrum very accurately due to a comparatively lower data length compared to the data length required, in order to obtain an acceptable frequency resolution. Therefore, as explained above, zero-padding is helpful to estimate the frequencies present in the signal more accurately.

From above, $T_{seg} = 0.12$ seconds, thus the true resolution is $(1/T_{seg}) = 8.33$ Hz. Typically, the signals were zero-padded to be 18 times as long as the data extract.

The focus of this research was to develop a method to estimate the bulk modulus during the transient cycle of the fuel system. The transient rail pressure signal obtained from the combined fuel system model also consists of pumping events every 90° and injection every 120°, as in the case of steady-state operation of the fuel system. However, this model can be modified, as has been seen in Chapter 2, to accommodate various pumping intervals. In the transient rail pressure signal, the rail pressure is not regulated to be around a constant pressure. This is because the Inlet Metering Valve (IMV) stays fully open until the system reaches a steady state. This in turn gives rise to an additional ramp component, which is absent in the steady-state data. Figure 3.10 demonstrates a transient rail pressure signal with pumping every 180° and no injections.

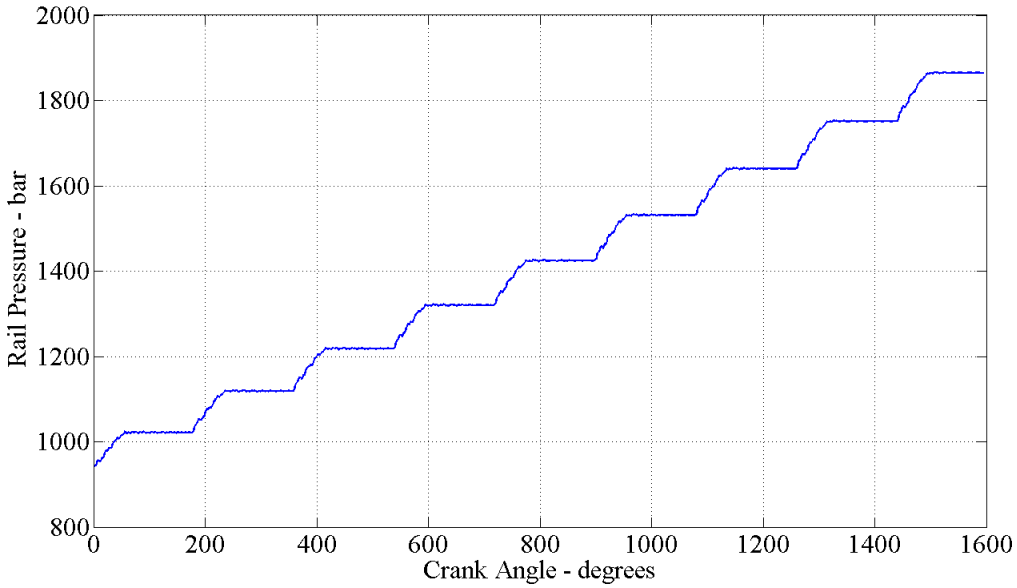

Figure 3.10. Rail pressure - no injections, pumping only with starting rail pressure of 950 bar at 1000 RPM.

The case with transient rail pressure data with pumping events every 90° and injection events every 120° has been considered to examine the frequency analysis.

- **Test Case**: In order to study the effect of having a ramp component in the rail pressure data, a test case is created that consists of two sinusoidal waves having frequencies close to pumping and injection frequencies, respectively. For ease of calculation, frequency values for the test case are chosen so that there are six complete injection events and eight complete pumping events in one cycle. The amplitudes of the sinusoidal waves are 160 units and 40 units, representing the amount of pressure rise due to pumping and pressure drop due to injection, respectively. The two sinusoidal waves are added to each other, imitating a steady-state simultaneous pumping and injection rail pressure signal, as shown in Figure 3.11. To this signal, a ramp of a specific equation is added. The transient rail pressure signal obtained from GT-simulations for one cycle and a starting rail pressure of 2400 bar is considered for obtaining the equation of the ramp signal. The equation is calculated by determining the equation of the line passing through the rail pressure data from simulations. The second subplot in Figure 3.12 demonstrates the test signal that imitates a clean transient rail pressure signal.

  The resulting signal looks like a clean transient signal containing similar frequencies as that of the transient signal obtained from GT-simulations. The single-sided magnitude spectrum of the test signal of this clean signal is obtained by using the fft (for fast fourier transform) in MATLAB, as shown in the first subplot in Figure 3.13. As can be seen in the figure, multiple frequency peaks are seen due to addition of the ramp. The second subplot in Figure 3.13 shows single-sided amplitude spectrum of the test transient waveform after subtracting the ramp component. As a result, distinct frequency peaks are seen at the injection and pumping frequencies.

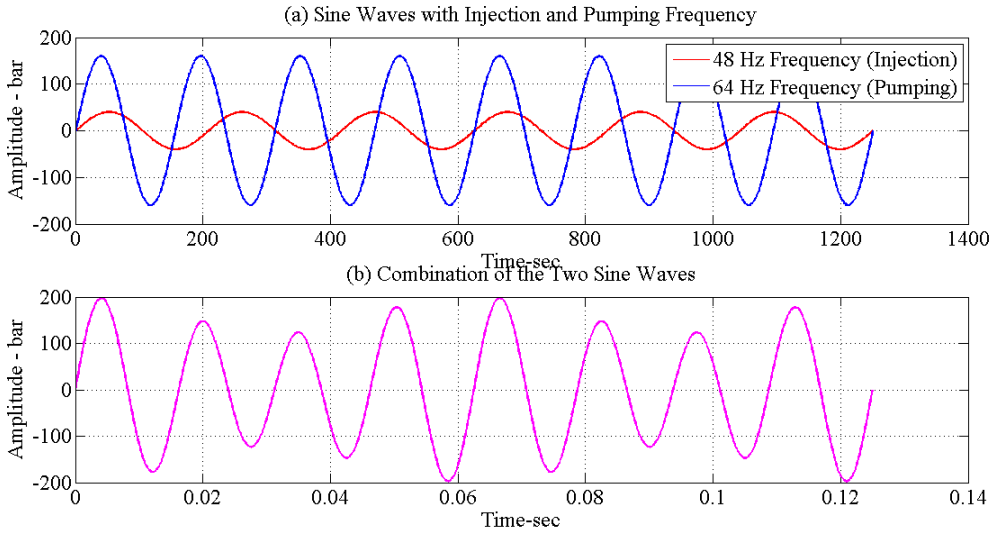

Figure 3.11. Simulation of test case showing sine waves imitating simultaneous pumping and injection. (a) Pumping (blue) and injection (red) components, and (b) the result of combining the two sine waves (pink).

This points to the fact that in order to be able to observe the frequencies of interest in real data, the frequency of the ramp component needs to be removed or suppressed. Therefore, to obtain a better frequency resolution of the rail pressure signal obtained from GT-simulations and to be able to view the frequencies that are not visible due to dominance of the ramp signal, such as the injection frequency, sufficient zero-padding is done to the data. The frequency resolution without zero-padding is 8 Hz. This frequency resolution is brought down to 0.5 Hz by zero padding the signal with eighteen times its original length. The ramp component is removed by using the "detrend" function in MATLAB so that the signal oscillates around the zero value. The function "detrend" is used to figure out the trend of the signal and remove it for FFT processing of the signal. The trend of the signal that is removed in this case is the ramp. The single-sided amplitude spectrum of this zero-padded signal without a ramp component gives dominant peaks at the injection and pumping frequencies, as expected, and the peak due to the ramp vanishes with the removal of the

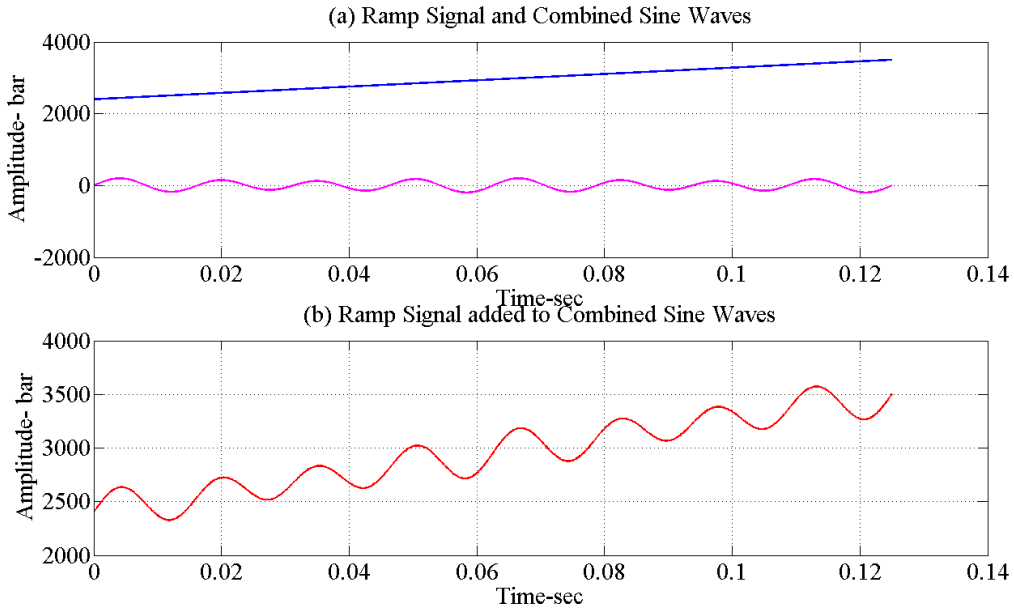

Figure 3.12. Simulation of test case imitating transient rail pressure.(a) Ramp (blue) and sinusoidal (pink) components, and (b) the result of combining the two components (red).

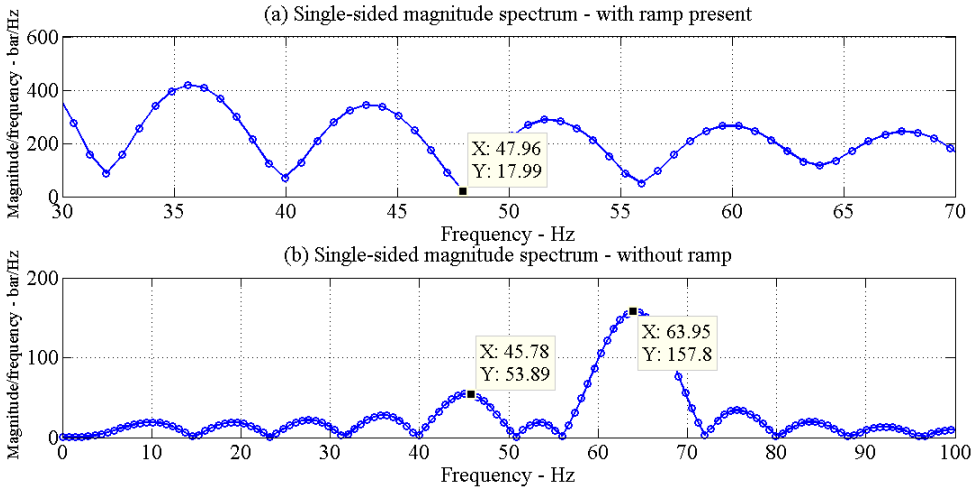

Figure 3.13. Single-sided magnitude spectrum of test data (a) with ramp component, and (b) without ramp component.

data. Figure 3.14 shows the frequency spectrum of rail pressure data from GT-simulations with 1000 bar starting rail pressure at 1000 RPM.

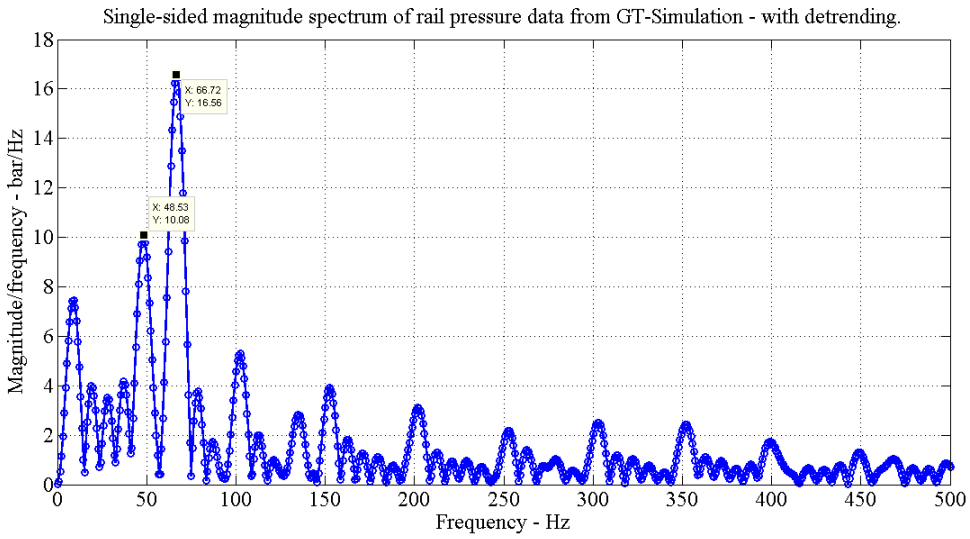

Figure 3.14. Single-sided amplitude spectrum of zero-padded transient GT data without ramp component at 1000 bar starting rail pressure and 1000 RPM with 90° pumping interval and 120° injection interval.

- **Variations in Ramp Component**

  In order to observe the effects of the ramp on the frequency spectrum in more detail, two variations in the ramp have been considered:

  1. Change in the slope of the ramp signal.
  2. Change in the data length considered.

  Figure 3.15 shows the single-sided magnitude spectrum of ramps of the same data length with slopes of 10, 500, 1000 and 1500 in subplot 1. It can be seen that increase in slope causes an increase in amplitude of the single-sided magnitude spectrum. A direct inference of this is that if the rise due to pumping increases, the peak at the ramp frequency in the single-sided magnitude spectrum of the rail pressure signal increases in amplitude, making it difficult to observe the frequencies of importance.

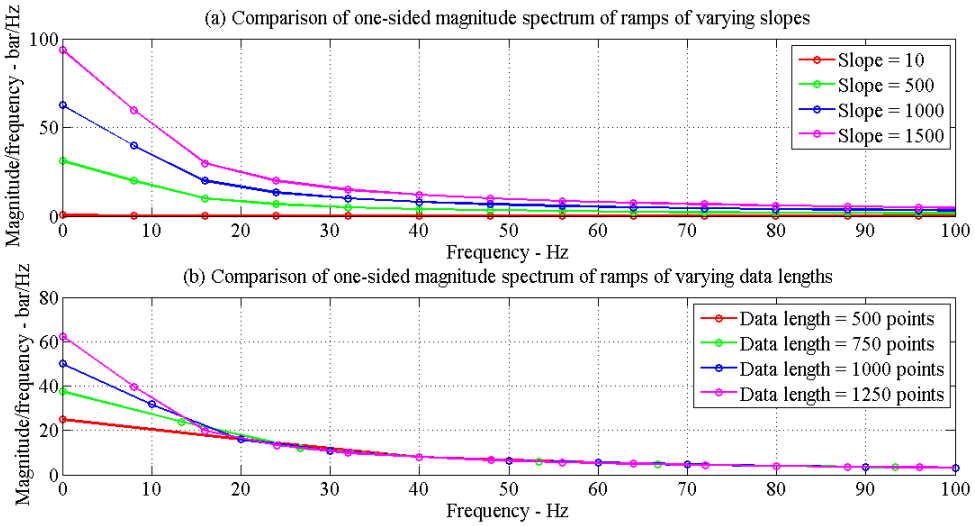

Figure 3.15. One-sided magnitude spectrum for various ramps. (a) Effect of the slope of ramp varying from 10 bar/sec (red) to 1500 bar/sec (pink). Length of data transformed was 0.125 seconds (=500 points). (b) Effect of data length with lengths varying from 500 points = 0.125 seconds (red) to 1250 points = 0.3125 seconds (pink). Slope = 500 bar/sec.

Figure 3.15 shows the single-sided magnitude spectrum of ramps of different data lengths with the same slopes in the second subplot. Data lengths of 500, 750, 1000 and 1250 data points are considered here. There is an increase in magnitude of the peak frequency with increase in data length. Since the bulk modulus estimator can take in only a limited number of data points at a certain time, it is necessary to know the effect of data length on the single-sided magnitude spectrum. This test highlights the fact that if high data length is considered for bulk modulus estimation, there is a need for zero-padding in order to increase the frequency resolution and be able to observe the frequencies of interest.

3.4 Filtering

Filtering the rail pressure signal is an important step towards determining the average pressure rise due to pumping. As the rail pressure signal obtained from the rail pressure sensor is noisy, and consists of high-frequency oscillation due to the dynamics of the rail, the signal is not clean enough to be directly used for pressure rise estimation. Filtering removes or suppresses unwanted frequency components.

The two main types of filters are the Finite Impulse Response (FIR) filters and the Infinite Impulse Response (IIR) filters, which are discriminated on the basis of the duration of the impulse response of the digital filter. The work in this research is based on filtering using the FIR filter. As FIR filters are always stable, they have been used for filtering of data during the course of this research. However, there is potential in exploring IIR filters for future work due to advantages like lower filter order.

3.4.1 Parks McClellan Low-Pass Filter

The Parks McClellan algorithm is a computationally-efficient and flexible method to design optimal FIR filters, and uses the Chebyshev algorithm for error approximation [19,20]. "In 1972, Parks and McClellan devised a methodology for designing symmetric filters that minimize filter length for a particular set of design constraints." [21] These design constraints include the pass-band and stop-band frequencies as well as the ripples in the pass and stop-bands. The computational effort of the Parks McClellan algorithm is linearly proportional to the length of the filter. "The resulting filters minimize the maximum error between the desired frequency response and the actual frequency response by spreading the approximation error uniformly over each band." [21]

To design the Parks McClellan filter in MATLAB, the "firpmord" and "firpm" functions are used. The filter order is estimated using the "firpmord" function and the filter is implemented using the "firpm" function.

The "firpmord" function takes as inputs the pass-band and stop-band edge frequencies, the pass-band and stop-band allowable ripple, and the sampling frequency. Based on these inputs, the function gives as its outputs the approximate filter order N, normalized frequency band edges F_o, frequency band magnitudes A_o, and weights W, which are used by the "firpm" function.

3.4.2 Identifying Frequencies of Interest

To give good enough pass band and stop band edge frequencies as inputs to the "firpmord" function, it is necessary to verify the frequencies of interest for the rail pressure data. Figure 3.14 shows the single-sided magnitude spectrum of the unfiltered rail pressure data, which includes the noise and oscillations due to rail dynamics. The rail pressure data is taken at pumping and injection intervals of 90° and 120°, respectively.

The method for choosing the pass-band and stop-band edge frequencies required as inputs to the "firpmord" function during the filter design process is as follows. First the injection and pumping frequencies are derived from the zero-padded signal frequency analysis (see the example in Figure 3.14). In this case, they are 66 Hz and 50 Hz, respectively. Thus, the end of the pass-band is set at 100 Hz. The choice for the stop-band is less clear. Two frequencies were considered: 200 and 300 Hz.

A lower stop-band edge results in a tighter filter, resulting in a higher filter order. The transient initialization due to filtering accounts for a transient portion of the same number of samples as the order of the filter. Therefore, the lower the stop-band edge frequency, the higher is the filter order, resulting in a greater effect on

the magnitude spectrum of the filtered data. This effect of the transient portion is visible in Figures 3.16 and 3.17 through change in magnitude of frequency peaks before the cut-off frequency. The magnitude spectra of data after filtering with filters with 200 Hz, 300 Hz and 1000 Hz stop-band edge frequencies are shown along with the magnitude spectrum of unfiltered data in Figures 3.16 and 3.17, respectively. In this case, the data was zero-padded 18 times longer than the original data length so that the locations of the peaks of the underlying sinc functions could be assessed more accurately.

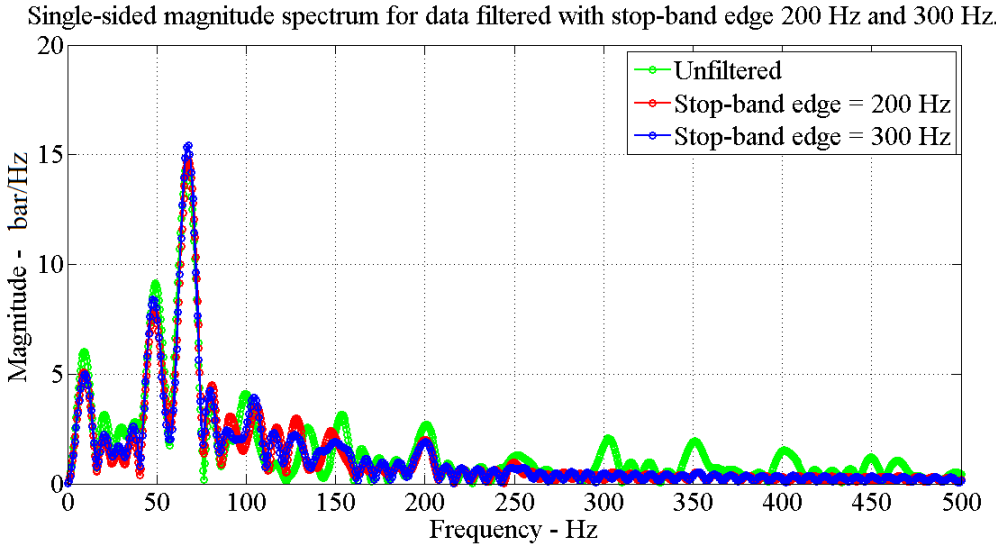

Figure 3.16. Single-sided magnitude spectrum of Parks McClellan low-pass filtered and zero-padded transient rail pressure data from GT-Simulation, without ramp component at 1000 bar rail pressure and 1000 RPM with 200 Hz and 300 Hz as stop-band edge frequencies.

There is a noticeable difference in the magnitudes of frequency peaks of filtered and unfiltered data sets before the cut-off frequency, which is 100 Hz, in Figure 3.16. However, the frequency peaks of data filtered with a filter of 300 Hz stop-band edge are closer in magnitude with the corresponding peaks of the spectrum of unfiltered data as compared to data filtered with 200 Hz stop-band edge. This is due to the lower

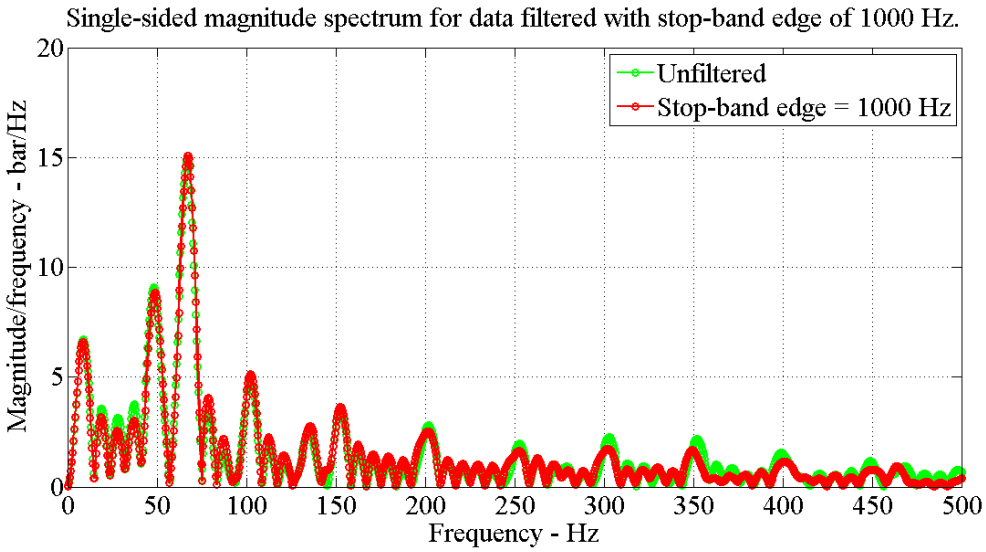

Figure 3.17. Single-sided magnitude spectrum of Parks McClellan low-pass filtered and zero-padded transient rail pressure data from GT-Simulation, without ramp component at 1000 bar rail pressure and 1000 RPM with 200 Hz and 300 Hz as stop-band edge frequencies.

filter order and, as a result, a lesser effect of transient initialization. This relation of filter order and transient initialization effect is further confirmed by Figure 3.17, where the magnitude spectrum of data filtered with a filter of 1000 Hz stop-band edge frequency is compared with that of unfiltered data. The filter order of this filter is very low compared to the previous two filters and, hence, there is closer matching between corresponding frequency peaks of filtered and unfiltered data. The drawback of using this filter, however, is that unimportant frequencies before 1000 Hz are retained, therefore, not giving a clean signal for our analysis.

It can be seen that the frequency spectrum for stop-band edge frequency of 200 Hz in Figure 3.16, gives a better filtered frequency response as compared to the frequency response of filtered output with 300 Hz stop-band edge. All the additional frequency components that are greater than 200 Hz are filtered out by the filter with 200 Hz as stop-band edge, whereas unimportant frequencies between 200 Hz and 300 Hz are

retained when the filter with 300 Hz as stop-band edge is used. In this research, 200 Hz has been used as the stop-band edge of the filter.

3.4.3 Scaling of Filtered Data

Data filtered with the "filter" function is observed to have a non-zero gain at zero frequency, when compared to the unfiltered data. Figure 3.18 shows the magnitude response of a Parks McClellan low-pass filter with pass-band and stop-band edge frequencies of 100 Hz and 200 Hz, respectively.

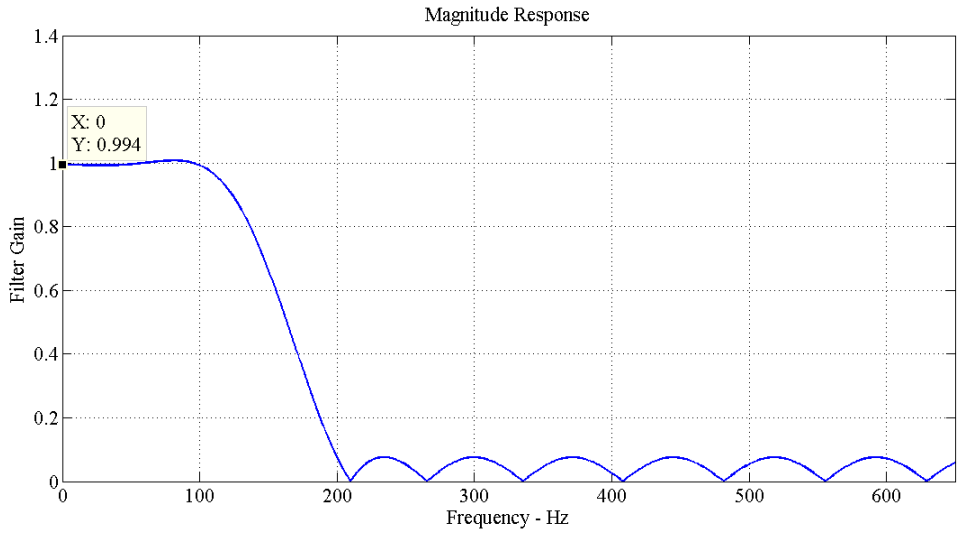

Figure 3.18. Magnitude response of a Parks McClellan low-pass filter for pass-band edge frequency of 100 Hz, stop-band edge frequency of 200 Hz and filter order = 135.

The gain at zero frequency, as shown by the data cursor, is -0.052 dB, instead of 0 dB. This gain is observed due to allowable ripple variation specified at the time of filter design. The gain of the FIR filter at zero Hz frequency is the sum of its coefficients. This can be verified by the following mathematical calculation:

FIR filter equation can be written as:

$$y_k = \sum_{i=0}^{N} b_i u_{k-i} \tag{3.6}$$

where b_i are FIR filter coefficients and u_{k-i} is the input to the FIR filter.

At zero frequency, z = 1. Therefore, at zero frequency, the gain of the filter can be written as,

$$\frac{Y(z)}{U(z)} = b_0 + b_1 + b_2 + ... + b_N \tag{3.7}$$

This suggests that the filtered data needs to be scaled by dividing it by the sum of all filter coefficients. Figures 3.19 and 3.20 show the test rail pressure data filtered with various ripple variations without scaling and with scaling of the filtered coefficients, respectively.

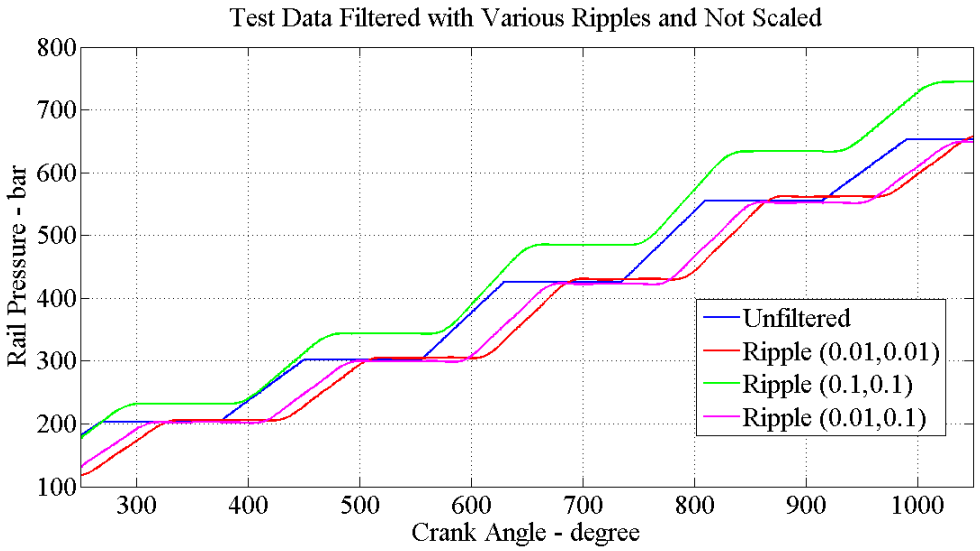

Figure 3.19. Filtered test rail pressure data without scaling of filter coefficients. Figure shows test data filtered using ripples of [0.01, 0.01] (red), [0.1, 0.1] (green), [0.01,0.1] (pink) and unfiltered data (blue).

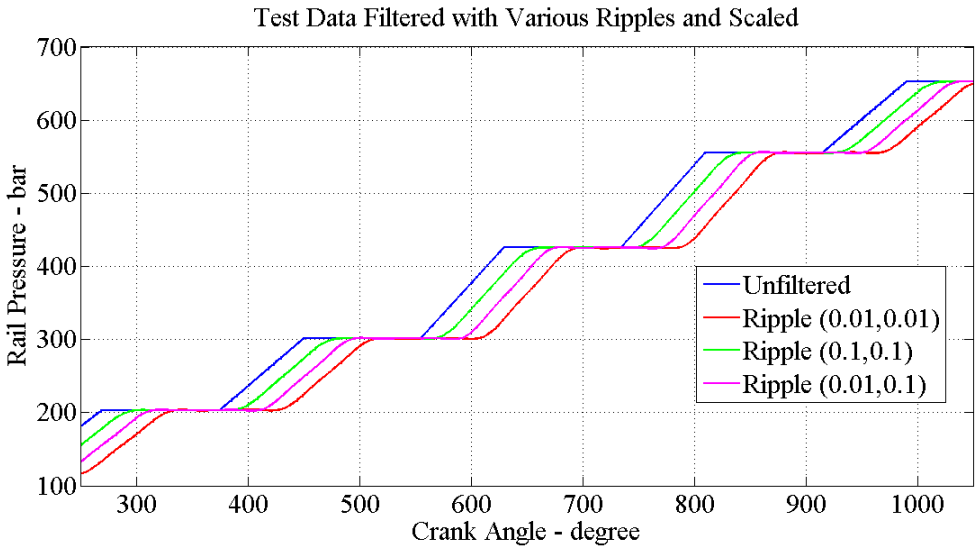

Figure 3.20. Filtered test rail pressure data with scaling of filter coefficients. Figure shows test data filtered using ripples of [0.01, 0.01] (red), [0.1, 0.1] (green), [0.01,0.1](pink) and unfiltered data (blue).

It can be seen from Figures 3.19 and 3.20 that the scaling causes the filtered waveforms to line up as expected. Scaling of filter coefficients has therefore been applied throughout all the filtering of data in this thesis.

3.4.4 Ripple Selection

The gain in the pass-band can be allowed to vary slightly from unity. This variation in the pass-band is the pass-band ripple, or the difference between the actual gain and the desired gain of unity. Three pairs of pass-band and stop-band ripple combinations have been examined in order to find the acceptable pass-band and stop-band ripple.

A higher ripple variation gives a lower filter order but more deviation from the gain of unity. A lower ripple variation, on the other hand, gives a lesser deviation from the gain of unity. However, this is at the cost of a higher filter order. The

ripple cases that are considered are [0.1 0.1], [0.01 0.1] and [0.01 0.01], where the first number represents the ripple in the pass-band and the second number represents the stop-band ripple. However, it is important to note that the filter order is decided not only by the ripple specification, but also by the spacing between the stop-band and pass-band edge frequencies.

To test the accuracy of the allowable ripples in the pass-band and the stop-band, test data resembling the transient rail pressure waveform has been created. The test data is filtered with a Parks McClellan filter with a pass-band edge frequency of 100 Hz, stop-band edge frequency of 200 Hz, and variations in the ripples in the pass-band and stop-band. Three cases of pressure rise between two points on each of the filtered waveform are compared to the actual pressure rise on the unfiltered waveform. The delay due to filtering in each of the filtered cases is considered so that the corresponding pressure rise is considered.

The delay due to filtering with an FIR filter is given by [22]:

$$Delay = \frac{(N-1)}{2} \quad \text{points} = \frac{(N-1)}{2} \times 0.1 \quad \text{msecs} \tag{3.8}$$

where N is the filter order of the FIR filter.

For example, the filter order with ripples [0.1 0.1] is 71 given by the "firpmord" function. This gives a delay of 35 points between the filtered waveform and the unfiltered waveform. The sampling rate is 10 kHz. Table 3.1 gives a summary of the filter order and delay caused by each of the ripple specifications.

Table 3.1. Summary of filter order and delay due to ripple specification.

Ripple	Filter Order	Delay
[0.1 0.1]	71	35 points
[0.1 0.01]	135	67 points
[0.01 0.01]	195	97 points

Each of the filtered waveforms in Figure 3.20 is checked for pressure rise estimate at certain crank angles. The comparison of pressure rise is done at the crank angles corresponding to the crank angles at which the pressure rise start point is considered for the unfiltered waveform. Table 3.2 gives a summary of three cases of pressure rise values that are considered at three different instances of crank angle for all the three ripple cases.

Table 3.2. Effect of ripple specification on pressure rise estimates.

	Accurate Pressure Rise	Ripple [0.1 0.1]	Ripple [0.01 0.01]	Ripple [0.01 0.1]
Set 1	98 bar	94.4 bar	95.4 bar	96.5 bar
Set 2	106 bar	102.1 bar	102.7 bar	104.7 bar
Set 3	130 bar	124.8 bar	126.2 bar	127.5 bar

It can be seen from the table that the most accurate pressure rise is given by the case where the ripple is [0.01 0.1]. This ripple specification has been used to filter all the data in this thesis while estimating the bulk modulus.

3.5 Pressure Rise Estimation

An important step in bulk modulus estimation is the determination of accurate pressure rise due to pumping. Rail pressure data consists of six injection events and eight pumping events over the course of one cycle, which is 720° revolution of the crank shaft. For steady-state data, it thus becomes necessary to identify the pressure rise due to clean pumping events, i.e., the pumping events not occurring around injection events. However, in the case of transient rail pressure events, the injections can be turned off by sending a signal from the ECM. The de-energizing of the injectors shuts off the injectors, giving a rail pressure signal consisting only of pumping events. The

approach used to detect the pressure rise is outlined in section 3.5.1. Figure 3.21 shows a transient rail pressure signal consisting of only pumping events.

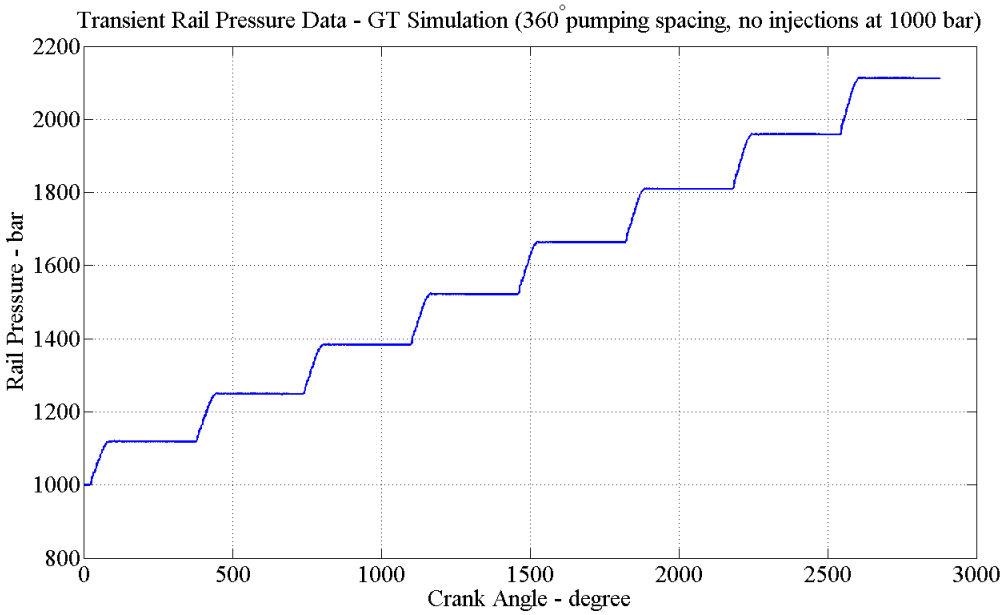

Figure 3.21. Transient rail pressure data from GT-Simulation with 1000 bar starting rail pressure at 1000 RPM, no Injections, 360° pumping interval.

3.5.1 One Moving Window Approach

The one moving window approach, as the name suggests, uses a single window that moves along the length of the signal. Figure 3.22 illustrates one window moving along the filtered transient rail pressure data consisting of only pumping events.

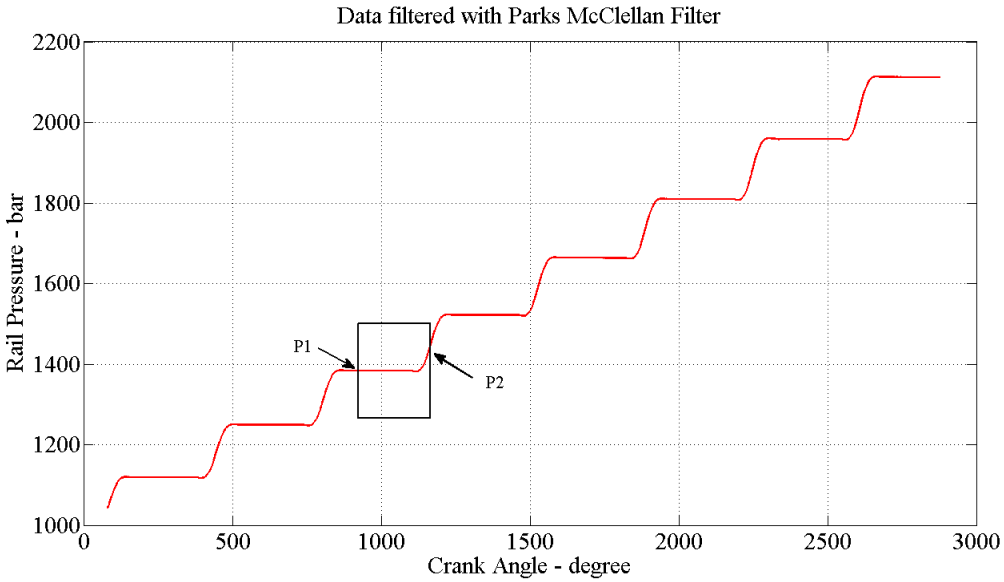

Figure 3.22. One moving window approach for filtered rail pressure data.

The window length is specified in terms of crank angle degrees. The interval between two pumping events and the average duration of the pumping events determine an acceptable range of window lengths that can be used to obtain the accurate pressure rise estimates. This will be discussed in detail in Chapter 4.

The difference between the pressure at the first point and the last point of the window when moved along the pressure rise signal gives a difference in pressure. Figure 3.23 illustrates the plot generated by moving a window of fixed length along the filtered rail pressure signal and plotting the difference between the pressure at the first and last points of the window. The window length used as an example is 156°.

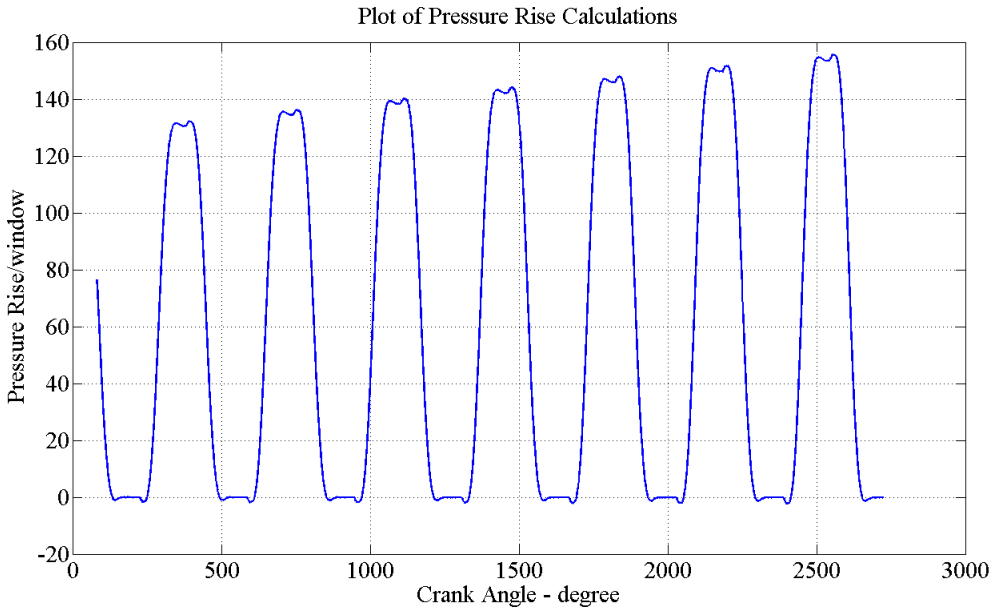

Figure 3.23. Pressure rise waveform generated from one moving window approach with a window length = 156°.

In Figure 3.23, the pressure rise produced by each of the pumping events is shown. For every pumping event, there is one estimate of pressure rise that represents the maximum pressure rise due to that particular pumping event. This peak pressure rise corresponds to the maximum difference between the first and last points of the window at that instant and is given by:

$$\Delta P = \text{Max}(P_2 - P_1), \tag{3.9}$$

where P_1 and P_2 are the pressures at the start point and the end point of the window, respectively.

The index of this maximum pressure rise from every pumping event is used to calculate the most accurate pressure rise estimate based on the window length and filter characteristics for that particular pumping event. This technique is explained

in detail in Chapter 4. The ΔP estimate obtained from every pumping event is then used to calculate the bulk modulus corresponding to the rail pressure at which that particular pumping event began. Considering multiple events for bulk modulus calculation gives a trend of bulk modulus vs. rail pressure for a particular fuel. Figure 3.24 shows the pressure rise estimates that have been computed from the data in Figure 3.23.

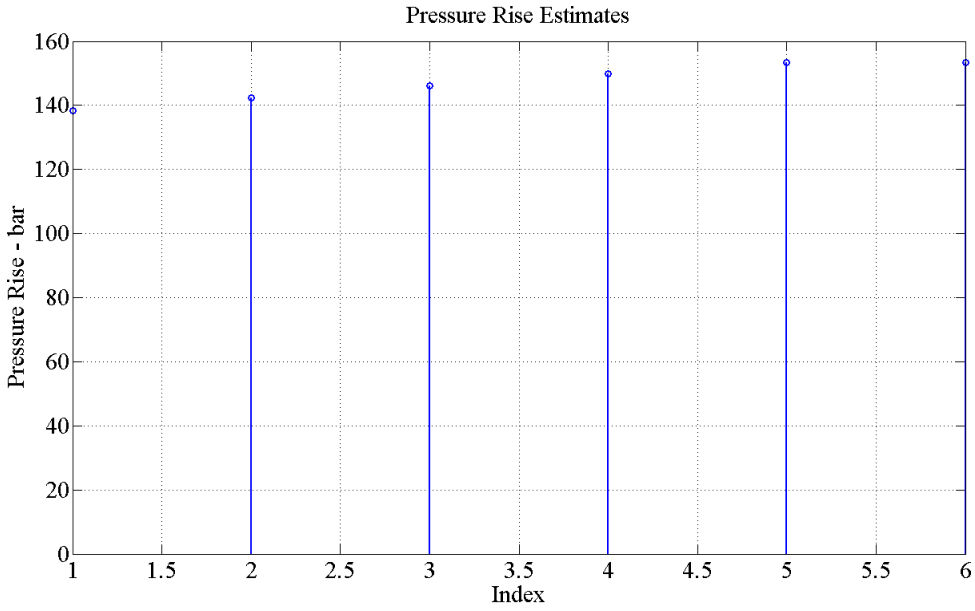

Figure 3.24. Pressure rise estimates generated from pressure rise data.

3.5.2 Summary of Pressure Rise Estimation

The outline of steps involved in pressure rise estimation can be written as follows:

1. Obtain filtered rail pressure data.
2. Select a good window length.
3. Move the window over the filtered rail pressure signal.

4. Simultaneously calculate the difference between pressure at the first and the last points of the window. This difference is the pressure rise estimate at each point on the rail pressure signal.

5. Examine the pressure rise estimates from every pumping event to find one maximum pressure rise value from each event.

6. Calculate the accurate pressure rise estimate based on the maximum pressure rise, window length and filter characteristics according to the technique explained in chapter 4.

7. Use each estimate obtained from every pumping event to calculate bulk modulus estimates of the fuel with respect to the rail pressure.

The bulk modulus estimation algorithm in this chapter throws light upon the various steps involved in calculating a good estimate of bulk modulus, especially on the detection of the pressure rise estimates. A detailed analysis of a good window length to be used, the effects of filter on pressure rise estimate, and error analysis is done in the following chapter.

4. PRESSURE RISE ESTIMATION

The pressure rise detection algorithm discussed in section 3.5 is to be applied to the rail pressure data obtained from GT-Suite simulations from which the bulk modulus is calculated. However, as the actual pressure rise due to pumping is not known, there is no means of verifying if the algorithm is accurate or not. This is because the rail pressure data from GT-Suite includes oscillations due to rail dynamics and the exact value of increase in pressure cannot be easily determined. In order to be able to study the effects of filtering, windowing lengths and pumping intervals, test cases with specific amounts of pressure rise have been created. This chapter describes ways to create such test rail pressure data sets and provides observations about windowing length and effects of filtering after applying the pressure rise detection algorithm. The observations from this chapter have been applied on rail pressure data from GT-simulations and Cummins test rig data to estimate the bulk modulus.

The method to create test rail pressure data and observations related to filtering and window length on ΔP estimation are discussed in section 4.1 of this chapter. Sections 4.2 and 4.3 summarize the results of bulk modulus estimation after observations from section 4.1 have been applied on data from GT-simulations and Cummins test rig, respectively.

4.1 Rail Pressure Test Data

To remove the oscillations, data is filtered and the one moving window approach is applied to it to determine the pressure rise ΔP. The type of filter used and windowing length have an effect on the estimation of ΔP. This helps in two ways:

1. The exact pressure rise due to pumping is already known, which makes it easy to test the pressure rise detection algorithm.

2. Several cases of pumping intervals can be tested before applying the algorithm on more realistic data.

4.1.1 Creating Rail Pressure Test Data

A clean transient rail pressure signal resembles an integrated series of pulses of varying amplitudes but same duration. This resemblance has been used to create the test data.

A stream of eight pulses, corresponding to one complete cycle, have been created. The on-time of each pulse is equal to the pumping duration. The pumping duration considered for the test data is 75°. The interval between the pumping events is varied from 90° to 360° according to the test case that is of interest. The amplitude of each pulse is calculated so that the area under each of the pulses equals the amount of pressure rise due to a single pumping event. For simplicity, these pressure rise values have been taken from the rail pressure data by running the GT-simulation model at 1000 bar with a starting rail pressure at 1000 RPM. These values include the influence of pressure drop due to injections as the data from GT-simulation includes simultaneous pumping and injection.

Figures 4.1 and 4.2 outline the steps to create test rail pressure data. Pulses in Figure 4.1 are integrated to give the plot in Figure 4.2.

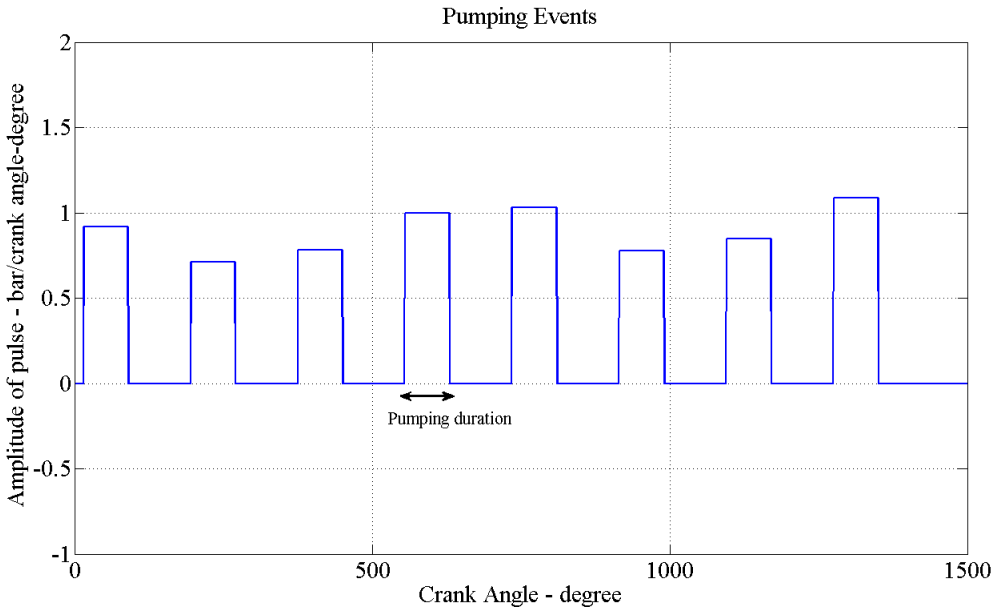

Figure 4.1. Pulses used to create test rail pressure waveform.

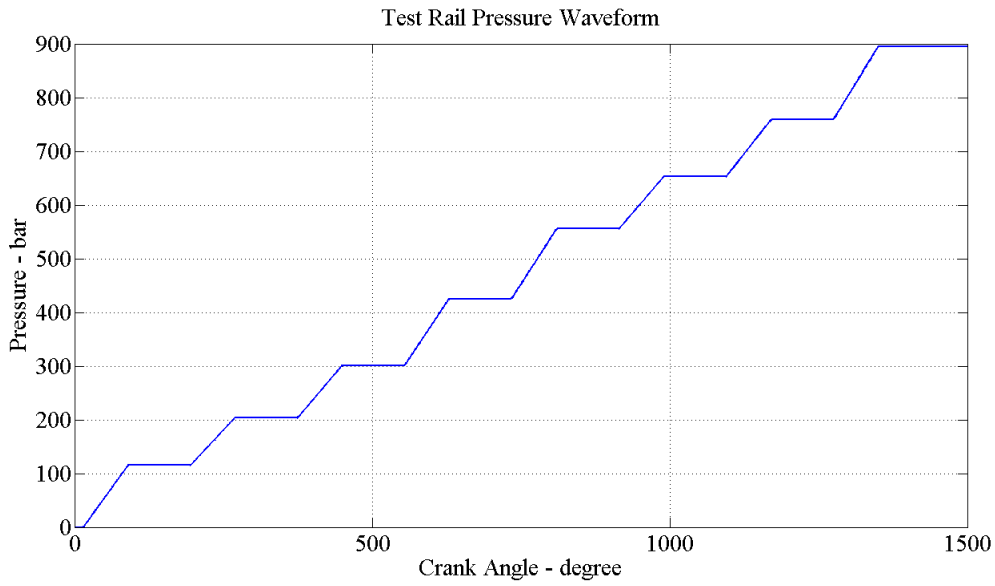

Figure 4.2. Test rail pressure waveform.

4.1.2 Observations on Effect of Filtering

This section discusses in detail the effects caused due to filtering on ideal test case of rail pressure data and their result on obtaining accurate pressure rise estimates.

- **Filtering the Data**: Filtering of data causes delay as discussed in Chapter 3. When test rail pressure data is filtered, as shown in Figure 4.3, the sharp edges become smooth. As can be seen in Figure 4.3, this causes the transition between the flat region and the slope to increase in time duration and also to become slightly round around the edges.

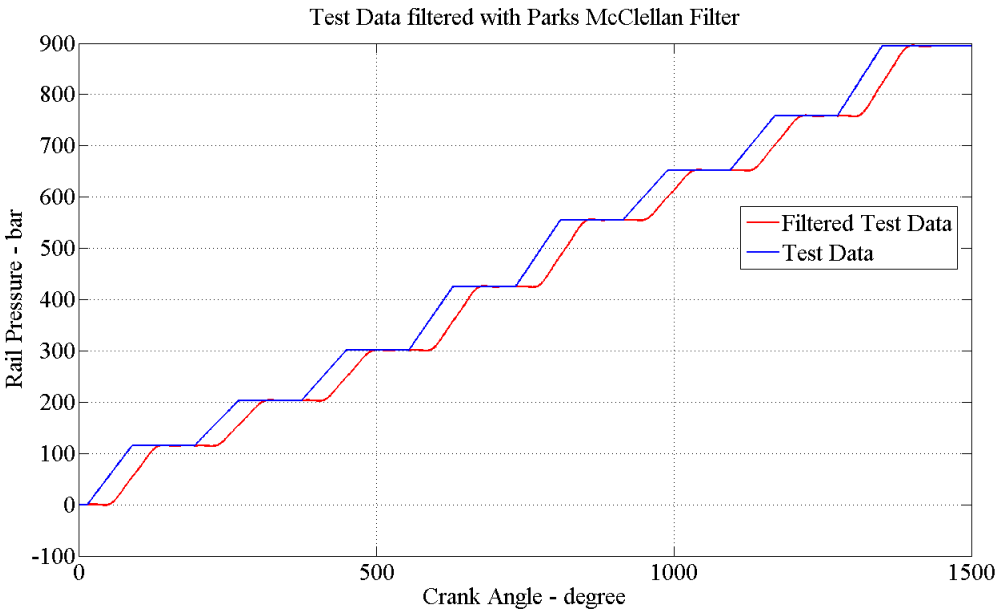

Figure 4.3. Effects of filtering the rail pressure data with 180° pumping interval and 75° pumping duration.

Figures 4.4, 4.5 and 4.6 show the pressure rise plots after moving windows of lengths equal to 81°, 132° and 174° of crank angle have been passed over the filtered test rail pressure data shown in Figure 4.3. It can be seen that the length of constant pressure rise in each of the discrete sections increases with the

length of the window. The constant pressure rise is seen to be equal to the actual pressure rise given in the test data. This is verified by checking the values in the constant pressure rise region through MATLAB. Another observation concerns the number of pressure rise points that are not equal to the accurate pressure rise, starting from the highest pressure rise in that pumping event. It has been observed that this length is equal to 28.8° of the crank angle, or 48 inaccurate pressure rise estimates on either side of the accurate pressure rise estimates (see Figure 4.6). This length is a property of the filter specification used and has been observed to change with change in filter specifications.

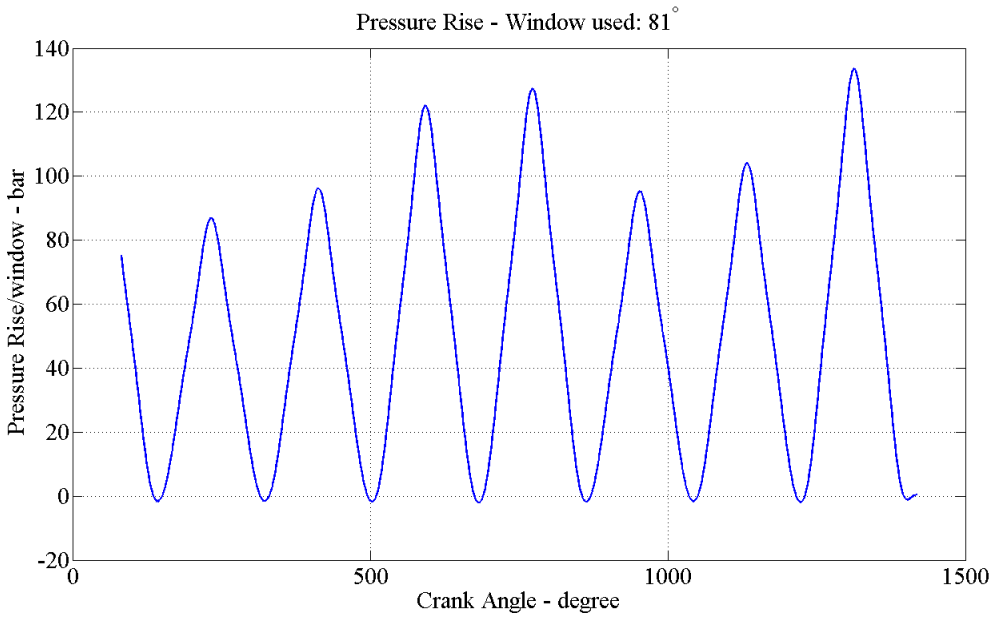

Figure 4.4. Pressure rise plot with window length = 81° with 180° pumping interval and 75° pumping duration.

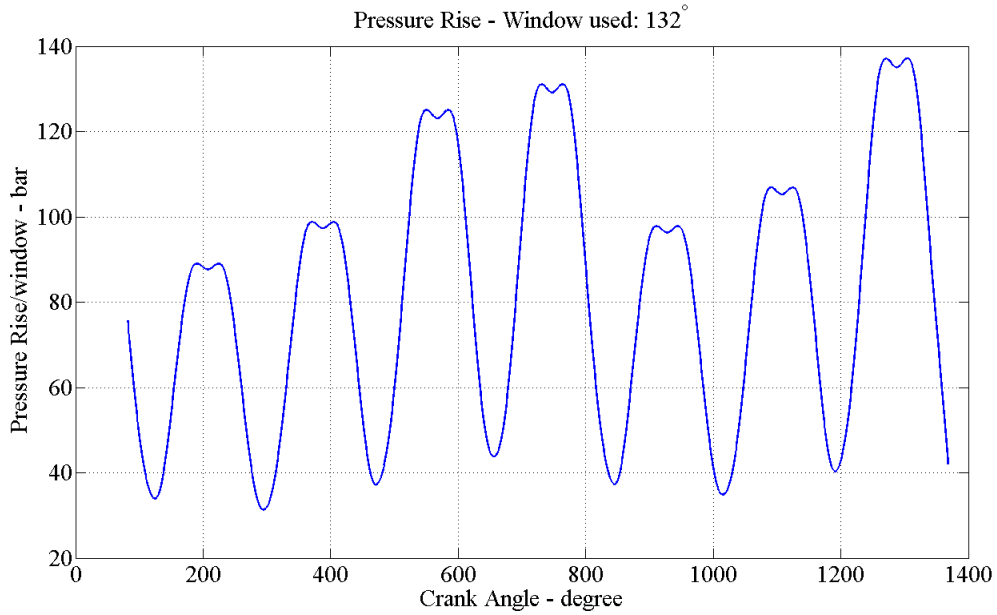

Figure 4.5. Pressure rise plot with window length = 132° with 180° pumping interval and 75° pumping duration.

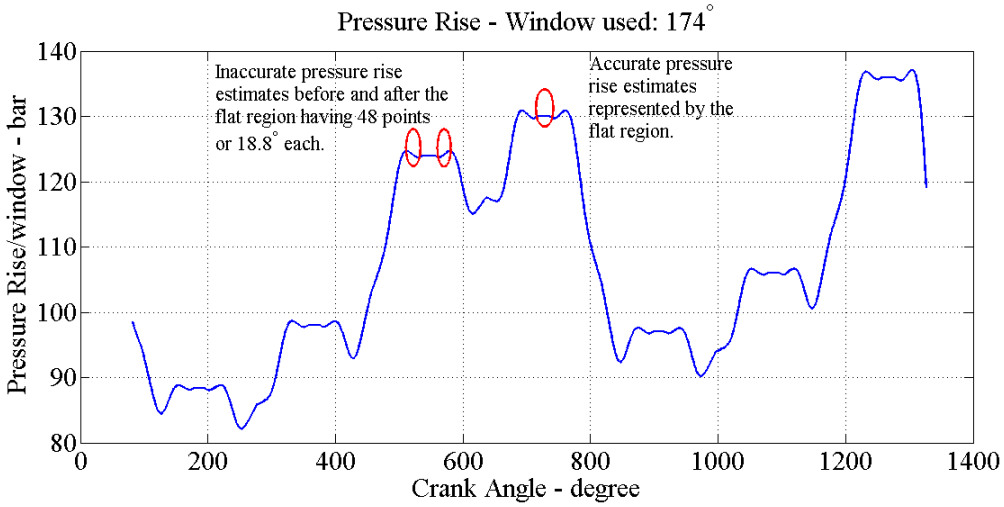

Figure 4.6. Pressure rise plot with window length = 174° with 180° pumping interval and 75° pumping duration.

From Figure 4.6 it is clear that there is a fixed number of points between the maximum pressure rise and the start of accurate pressure rise estimates, based on filter characteristics. Once the maximum pressure rise is detected from every pumping event as mentioned in Chapter 3, the index of this estimate is used to calculate the start of accurate estimates, which marks the beginning of the flat region in Figure 4.6. All the estimates in the flat region are then averaged to give a final pressure rise estimate for one pumping event. It is important to note that the accurate estimates are represented by the flat region only in the test case. This region will not be flat in case of data obtained from simulations or test rigs due to oscillations. However, the filter characteristics will still be the same and, hence, the number of points between the maximum pressure and start of accurate pressure rise region will be the same as in the test case, as will be the length of the accurate pressure rise region.

Studying multiple cases of window lengths and filtering specifications on the test case leads to the following relationship between pumping duration and minimum window length for estimating accurate pressure rise:

$$Window_{min} = \left(P + N \times \frac{360}{60} \times \frac{E_{speed}}{F_s} \right)^{\circ} \tag{4.1}$$

where $Window_{min}$ is minimum length of window in crank angle degrees to be used to obtain at least one point with accurate pressure estimate, P is pumping duration in degrees, N is filter order, F_s is sampling frequency in Hz and E_{speed} is engine speed in RPM.

Hence, using Equation (4.1), it can be concluded that for a pumping duration of 75° and a sampling frequency of 10 kHz, the minimum length of window is 156°. For a pumping duration of 51° and a sampling frequency of 10 kHz, the minimum window length to be used is 132°. This has been verified on the test data.

It is important to note here that an increase in the sampling frequency will increase the filter order by the same factor, therefore not having any effect on the minimum window length. Therefore, to change the minimum window length when sampling frequency is changed, without having to change the filter order, it is necessary to change the filter characteristics, such as the pass-band and stop-band edge frequencies of the filter. This theory has been applied while filtering data from the Cummins test rig, as will be seen in section 4.3.

- **Length of Window**: The number of accurate pressure rise estimates increases with an increase in the length of the window. These accurate pressure rise estimates can be averaged to give one estimate of pressure rise. As test data is clean and without any oscillations or noise, varying window lengths give the same value of pressure rise estimate since all the pressure rise estimates in the flat region of the pressure rise waveform give the same value of pressure rise as long as the window length is above the minimum window size required for at least one accurate pressure rise estimate. However, the window length is of importance while considering real data as all the pressure rise estimates would not be of the same amplitude. In that case, the higher the window length used, the better would be the pressure rise estimate.

  Figures 4.7 and 4.8 show the relationship between the length of window and number of accurate pressure rise estimates in the pressure rise waveform for 51° and 75° pumping duration. It is evident that for every one degree increase in the window length, there is an increase in the number of accurate pressure rise estimates by one, or in other words, the number of points in the flat region of the pressure rise waveform increases by one.

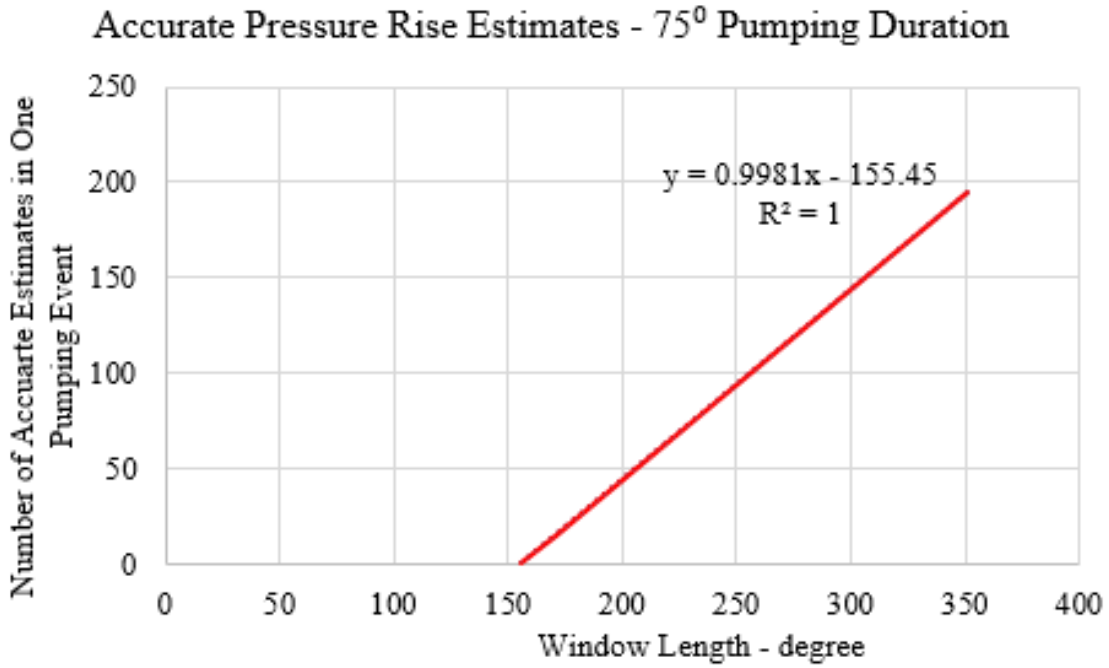

Figure 4.7. Number of accurate pressure rise estimates obtained vs. window length for 75° pumping duration.

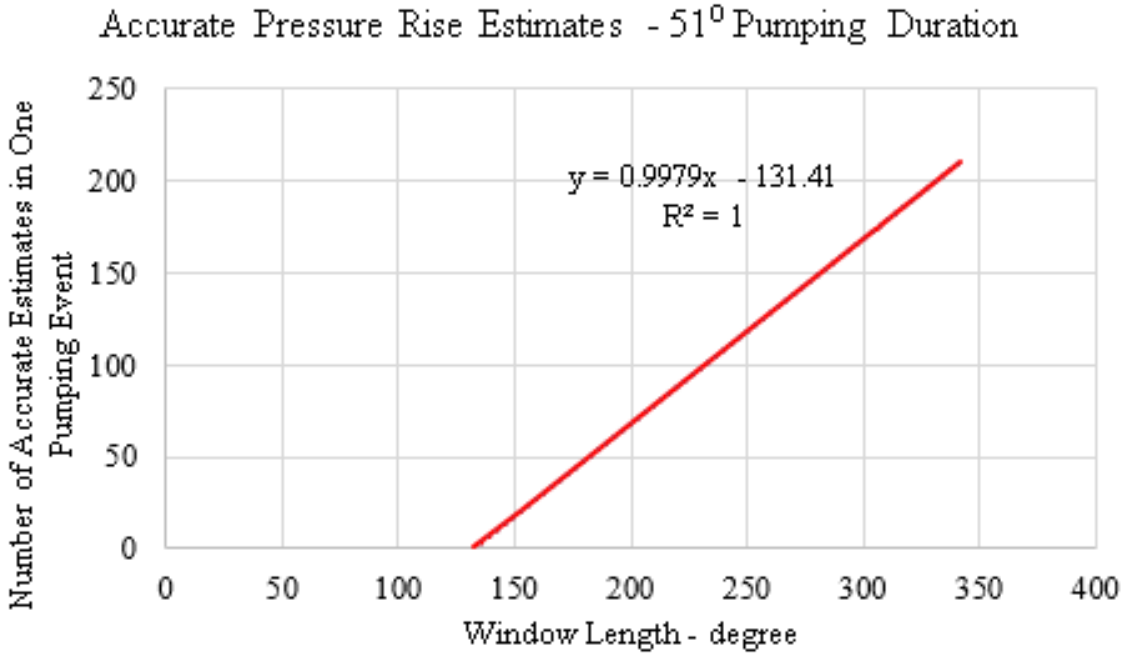

Figure 4.8. Number of accurate pressure rise estimates obtained vs. window length for 51° pumping duration.

The window length should be selected so that it covers the expanse of a single pumping event for pressure rise estimation. This means that the ΔP estimate from one pumping event should not have any influence from the previous or next pumping event. Therefore, there is an upper limit to the length of the window used, based on pumping duration and interval. Figure 4.3 shows filtered rail pressure data. As can be seen, the window would correctly capture all the rail dynamics for one pumping event if the window length extends from the beginning of a step to the beginning of the next step. If the window length goes beyond the beginning of the next step in the staircase waveform, it will capture rail dynamics from the next pumping event, causing error in the ΔP estimate. It was observed that beyond a certain window length, accurate pressure rise estimates are not obtained. Based on these observations, the maximum window length that can be used for a certain set of conditions is:

$$Window_{max} = \left(I - M \times N \times \frac{360}{60} \times \frac{E_{speed}}{F_s} \right)^{\circ} \tag{4.2}$$

where $Window_{max}$ is maximum length of window in crank angle degrees that can be used to obtain maximum number of accurate pressure rise estimates, I is pumping interval in degrees, N is filter order, F_s is sampling frequency in Hz, E_{speed} is engine speed in RPM and M is equal to 28 points for condtions with filter order of 135, sampling frequency of 10 kHz, engine speed 1000 RPM and pumping duration of 75°.

Equations (4.1) and (4.2) enable calculation of the desired pumping interval. The GT-Power pump model has an average pumping duration of 75°. This means that the minimum window length to be used needs to be 156°, for 1000 RPM and a filter order of 135 at sampling frequency of 10 kHz. Based on the cam displacement profile, the pumping intervals that can be used are 180° and 360°. For 180° interval in pumping, the maximum window length for accurate

pressure rise estimate would be 163.2°, based on Equation (4.2). For 360° interval in pumping, the maximum window length is 343.2° and minimum window length is 156°, which provides a total of 187.2° of data for averaging ΔP estimates. In order for rail pressure data with different specifications of pumping duration, pumping interval or filter specifications to be used, the sampling frequency or the engine speed can be changed, so that a usable window size for pressure estimation is obtained. An example of this type of manipulation is done in section 4.3, where rail pressure data from the Cummins fuel systems rig is tested.

4.2 Bulk Modulus Estimation - GT Simulation Data

The results obtained from the sections above are used to estimate the bulk modulus of D2 using rail pressure data obtained from GT-Simulation with pump spacing as 180°. The sampling rate is 10 kHz and the engine speed is 1000 RPM. The data from the simulation has the same nature as that of the test data described above with the addition of oscillations due to rail dynamics.

For simplicity, pressure rise from a single pumping event is considered for calculations. Rail pressure data is taken at starting rail pressures of 1000 bar, 1500 bar and 2000 bar. The pressure rise estimation algorithm is used to detect ΔP. Value of system volume, V, is calculated from the model in GT-Power, which is 0.14529 L. The value of ΔV is the simulated value of volume of fuel pumped out of the Outlet Control Valve into the rail.

Table 4.1 shows the values of pressure rise estimates due to a single pumping event starting at rail pressures of 1000 bar, 1500 bar and 2000 bar, in column 2, with the corresponding volume of fuel pumped into the rail, in column 3. These values, along with the value for system volume, are used in the isentropic bulk modulus formula

to estimate the bulk modulus at those pressures. Table 4.2 contains a comparison of the calculated bulk modulus values at 1000 bar, 1500 bar and 2000 bar, with the bulk modulus values from GT-simulation at those pressures by calculating the error between the two, with respect to the simulated values of bulk modulus. The difference between bulk modulus of D2 and B100 is roughly 7% [16], implying that the difference between D2 and B20, which is the most commonly used blend of biodiesel for transportation [11], is even lower. The error values in Table 4.2 suggest that the uncertainty associated with bulk modulus estimation for D2 may not be low enough to distinguish D2 from B20.

Table 4.1. Summary of bulk modulus estimation for GT-simulation data with 180° spacing at 1000 RPM.

Pressure (bar)	Δ P (bar)	Δ V (L)	V (L)	Estimated Bulk Modulus (bar)
1000	91.98	5.35×10^{-4}	0.145	24929.16
1500	110.90	5.22×10^{-4}	0.145	30805.56
2100	126.88	5.04×10^{-4}	0.145	36430.89

Table 4.2. Summary of errors for bulk modulus estimation from Table 4.1.

Pressure (bar)	Bulk Modulus from Simulation (bar)	Error (%)
1000	24854.33	0.30 %
1500	30061.20	2.47 %
2100	35939.79	1.37 %

4.3 Pressure Rise Estimation - Cummins Fuel Systems Rig Data

The pressure rise estimation algorithm is applied to rail pressure data that was collected by Cummins, Inc. The data was obtained at transient conditions with a starting rail pressure of 150 bar and ending pressure of 2800 bar. The engine speed was 1000 RPM and sampling rate was 1 MHz. The data is from a test rig that used Viscor (a diesel substitute). The pumping interval is 180° and, like the test data that we have seen in the previous sections, the rail pressure data did not involve any pressure drops due to injections.

Although this data is of value, the accurate pressure rise is unknown, due to the rail dynamics as well as sensor noise. As the sampling rate is much higher than the sampling rate of data obtained from GT-simulations, the test rig data needs to be downsampled in order to be filtered by a practically-realizable filter. The calculations for the downsampling and usable window length for pressure rise estimation are discussed in the following section. For simplicity, a single pumping event from the rig rail pressure data is considered for the application of the pressure rise estimation algorithm.

4.3.1 Filter Manipulation

To attain usable information from the rig rail pressure data, noise and oscillations need to be removed by a decent filter. The filter order plays an important role in determining the minimum window size that can be used to obtain accurate pressure rise estimates. Figure 4.9 shows a single pressure rise due to pumping.

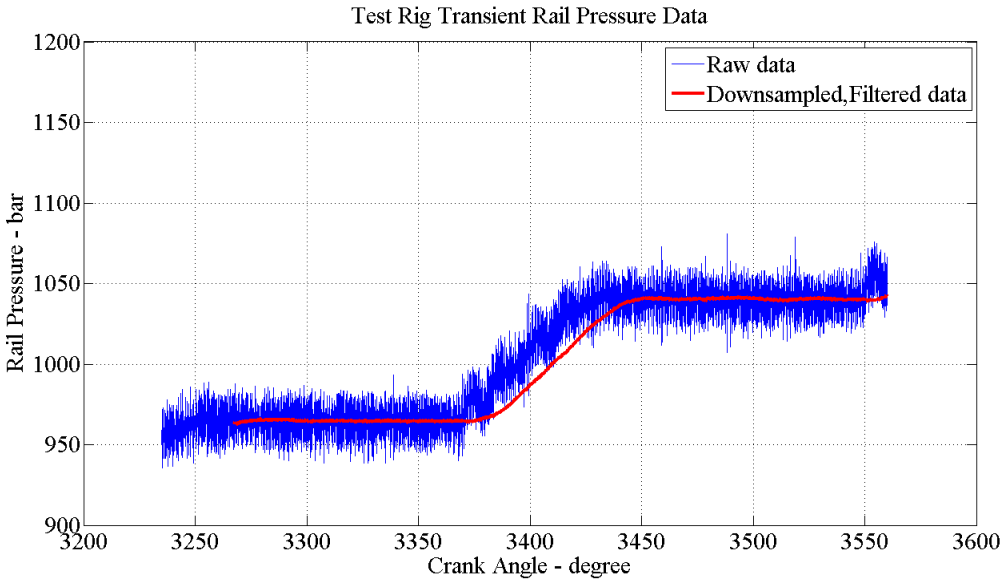

Figure 4.9. Test rig data pressure rise due to a single pumping event at 1000 bar rail pressure with 180° pumping interval.

In order to have a good estimate of ΔP, an appropriate number of pressure rise points need to be averaged, to get a mean pressure rise. However, the number of usable pressure rise estimates depends on the minimum and maximum window lengths used to obtain the pressure rise data points. The minimum window length, as seen in Equation (4.1), depends on the sampling frequency, filter order, pumping duration and engine speed, and the maximum window length, as seen in Equation (4.2), depends on pumping duration and pumping interval, as well as sampling frequency, filter order and speed. In the Cummins test rig data, the engine speed, pumping interval and pumping duration are known quantities.

The test cases described in previous sections have been filtered with a filter with order 135, which has yielded fair results. To continue using a filter with filter order of 135, the design parameters of the filter need to be changed accordingly. For previously-designed filters, the pass-band and stop-band edge gap is 100 Hz with a

ripple of 0.01 in pass-band and 0.1 in stop-band and a sampling frequency of 10 kHz. Therefore, we will downsample the test rig data from 1 MHz to 10 kHz.

Therefore, the original frequency of 1 MHz of the test rig data is downsampled by 100, to give a sampling frequency of 10 kHz. The filter order is retained to 135, like that of the filter that was used to filter test data, by setting the pass-band edge frequency to 40 Hz and stop-band edge frequency to 140 Hz.

Figure 4.10 shows the magnitude spectrum of the raw test rig rail pressure data without the ramp component. As expected, a peak is seen at the approximate pumping frequency, i.e., at 33.56 Hz. There are a few small frequency peaks seen after the pass-band edge of the filter, i.e., 40 Hz. The filter specifications can thus do a fair job of filtering out the unimportant frequencies. However, as the stop-band cannot be lower than 140 Hz due to constraint on filter order, direct control over frequencies between 40 Hz and 140 Hz is not achieved.

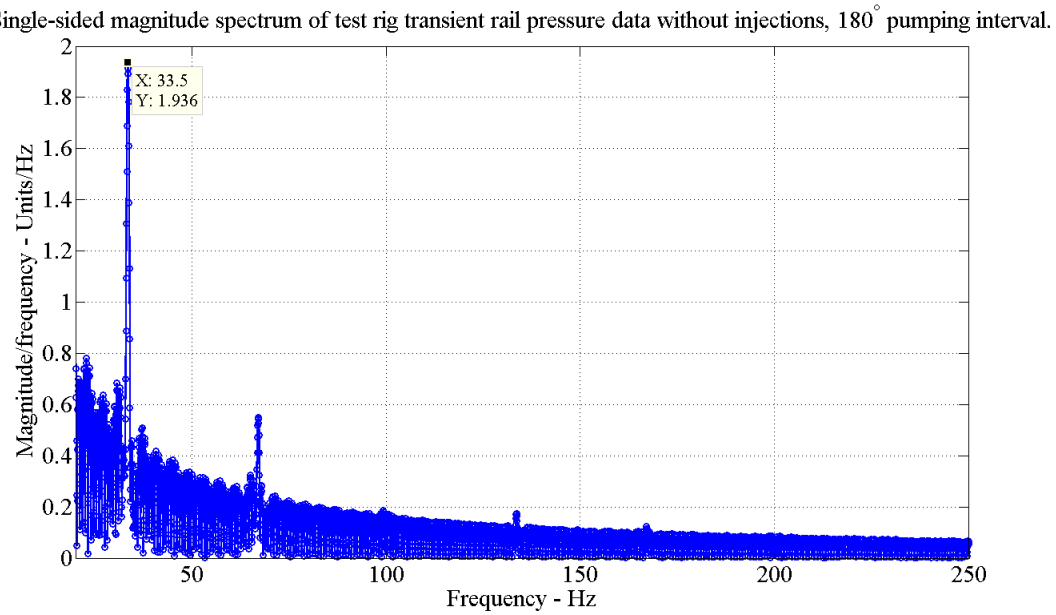

Figure 4.10. Single-sided magnitude spectrum of raw transient rail pressure test rig data with 180° pumping duration and no injections, without ramp component.

4.3.2 Pressure Rise Estimation

The best pressure rise estimate for the data is obtained when the maximum window size is used. Figure 4.11 outlines the steps involved in pressure rise estimation of the rail pressure data. The first sub-plot shows downsampled and filtered test rail pressure data. The second sub-plot demonstrates the pressure estimates obtained when a window of 162° is moved over the filtered data. The mean pressure rise estimate is shown in the third sub-plot.

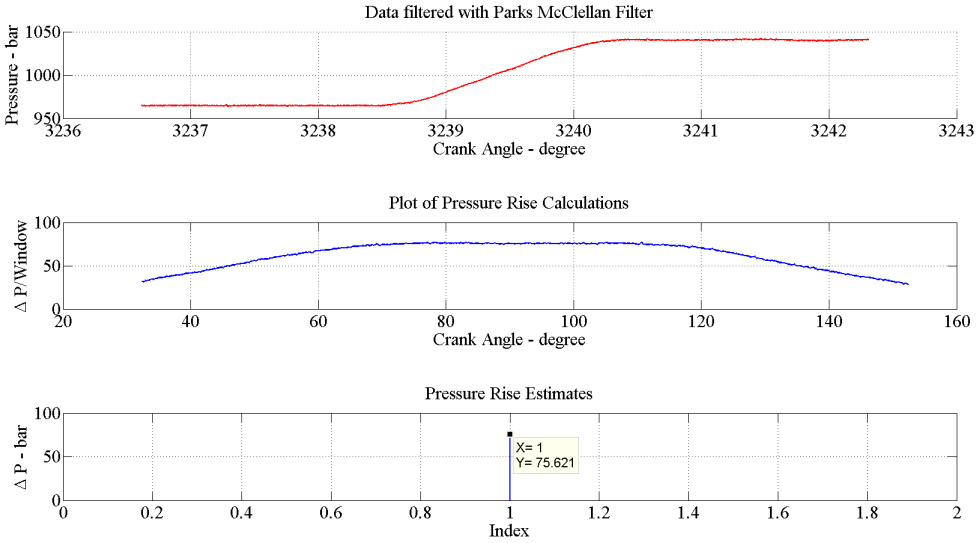

Figure 4.11. Pressure rise estimation of transient rail pressure filtered data window size = 162°.

Using a window of 162°, the ΔP estimate obtained is 75.621 bar, at a rail pressure of 1000 bar. The value of ΔP obtained from GT-simulation is 92 bar, as seen in section 4.2 at a pressure of 1000 bar. This difference in ΔP can be attributed to the difference in dimensions for bore diameter and stroke for the pump chamber in the GT-model and Cummins test rig. For the GT-model, the total mechanical

displaced volume is 651.27 mm^3. The mechanical displaced volume for the test rig is 527.78 mm^3. As the volume displacement in the pump chamber in the GT-model is greater than the volume displacement in the pump chamber from the test rig, it can be concluded that the pressure rise due to pumping would be greater in the rail pressure data from the GT-model. The ratio of displaced volume from GT-model to the displaced volume from the test rig and the ratio of the ΔP produced due to pumping from the two chambers at 1000 bar, is given below:

Ratio of displaced volume $= \frac{651.27}{527.78} = 1.23$

Ratio of pressure rise due to pumping $= \frac{91.98}{75.62} = 1.22$

The pressure rise from the rail pressure data from the test rig, therefore, needs to be scaled to match the pressure rise due to pumping from the GT-model in order to verify the accuracy of the results. Scaling the pressure rise estimate, we have $\Delta P = 75.621 \times 1.22$ bar $= 91.98$ bar. The system volume, V, as stated before, is 0.145 L and ΔV is $5.43 \times 10^{-4} L$ at 1000 bar rail pressure. These values for V and ΔV have been taken from GT-Simulation. The isentropic bulk modulus, therefore, is calculated as:

$\beta_{isentropic} = V \frac{\Delta P}{\Delta V} = 24984.45$ bar

The value of isentropic bulk modulus at 1000 bar for D2 from GT-simulation data is 24854.33 bar. The estimated isentropic bulk modulus, thus, gives an error of 0.5235% with respect to the bulk modulus estimate obtained from GT-simulation transient rail pressure data.

4.3.3 Bulk Modulus Dependence on Pressure

Bulk modulus linearly increases with increase in pressure. However, each fuel has a characteristic slope connected to the bulk modulus - pressure relationship [16]. The determination of this slope is another method to characterize a fuel. The rail pressure

data obtained from GT-simulations has been used to demonstrate the relationship of bulk modulus with rail pressure. Pressure rises due to pumping at varying rail pressures have been considered to calculate the bulk modulus at those pressures. The data for system volume and volume of fuel pumped out from the outlet check valve have been taken from GT-simulations. Figure 4.12 demonstrates the pressure dependence of bulk modulus values for D2 in comparison to pressure dependence of biodiesel based on the estimation algorithm and values obtained from GT-simulation. The biodiesel fuel object has been custom-defined in GT-simulation based on data compilation by Saboo in his research report [23].

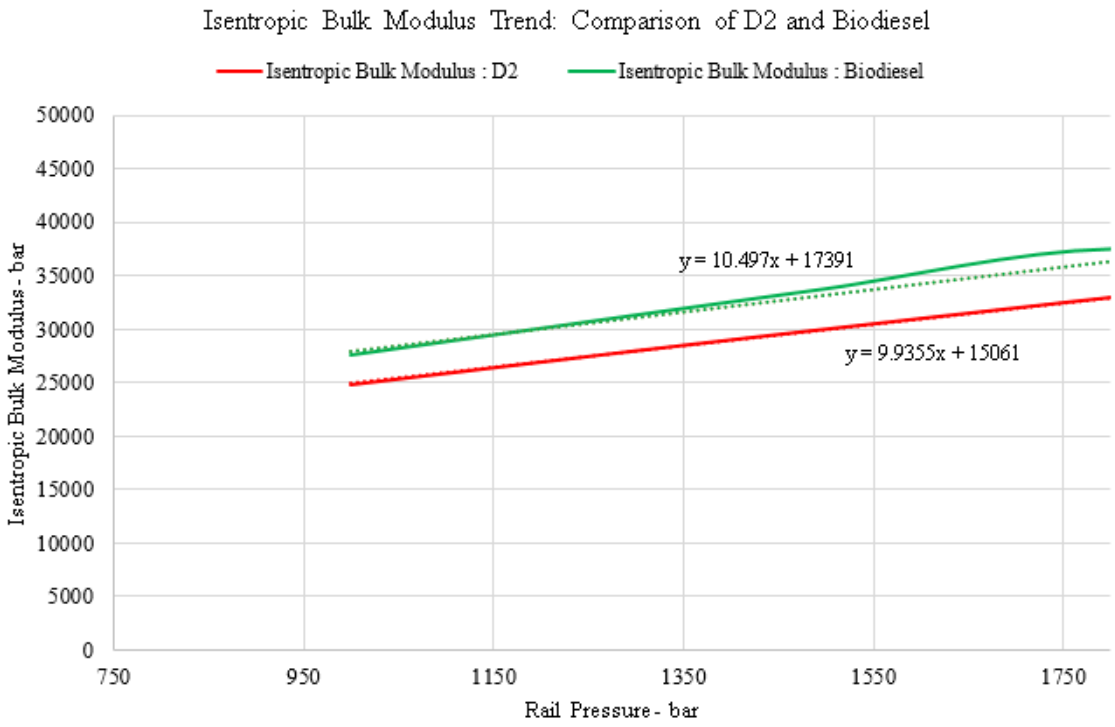

Figure 4.12. Variation of bulk modulus with rail pressure for D2 and Biodiesel based on rail pressure data from GT-simulations.

Table 4.3 shows the values of ΔP, ΔV and estimated bulk modulus for Cummins data for various starting rail pressures, ranging from 1000 bar to 2400 bar. The

system volume V is 0.145 L for all cases. Pump inlet temperature is controlled to 40° C.

Table 4.3. Variation of ΔP estimates and bulk modulus with rail pressure for Cummins rig data.

Rail Pressure (bar)	Scaled ΔP Estimate (bar)	ΔV (L)	Estimated Bulk Modulus (bar)	Error (%)
1000	92.36	5.35×10^{-4}	24984.45	0.71
1300	105.35	5.29×10^{-4}	28838.28	3.03
1500	111.35	5.22×10^{-4}	30895.00	2.89
1800	119.38	5.13×10^{-4}	33702.92	2.15
2100	127.40	5.05×10^{-4}	36538.28	1.78
2400	135.52	4.98×10^{-4}	39385.84	1.70

The bulk modulus estimates increase almost linearly with rail pressure, as seen in Figure 4.12. The slope of the trend line based on bulk modulus estimates matches closely with the trend line of bulk modulus values computed by GT-simulation. This provides an alternative approach to fuel type estimation. Rather than looking at the absolute values of bulk modulus for a particular fuel at a given pressure, a series of bulk modulus estimates can be computed at various pressures and the trend in the pressure dependence of bulk modulus can be observed to determine the fuel type.

The accuracy of bulk modulus estimates during the course of this research is tied with the accuracy of ΔP estimates as well as the value of ΔV, as both these values have errors associated with them. However, for the calculations in this research, the value of ΔV has been taken from GT-models and the error associated with it can be neglected for now. The bulk modulus is found as a function of pressure, and the

errors associated with the estimation are, therefore, calculated only taking the errors in ΔP into account. When errors in ΔV are included, the errors in estimation of bulk modulus would be larger and would make it difficult to determine the fuel type precisely. Assuming that there are no external factors affecting the properties of the fuel, the accuracy of bulk modulus estimate, in this case, can be quantified from the accuracy of pressure rise estimate it is calculated from. Knowing the accuracy of the bulk modulus estimates is important because the estimates are used to determine if the fuel type is diesel or biodiesel. The accuracy of the bulk modulus estimates, when compared with the difference between the bulk modulus estimates of diesel and biodiesel, will help determine the actual gap between bulk modulus values of the two fuel types.

5. CONCLUSIONS AND PROPOSED FUTURE WORK

The work presented in this thesis can be divided into three parts: fuel system modeling and simulation, analysis of the bulk modulus formula, and pressure rise and bulk modulus estimation techniques. These categories are described below, along with the contributions and proposed future work.

5.1 Summary

This research explores the method to determine bulk modulus of a fuel for fuel type determination, as a step towards adaptive injection control. Parameters such as fueling quantity, injector on-time and injection timing can be controlled if the fuel type is known, giving a better performance of the fuel system. The other parameters that distinguish one fuel type from the other are density, speed of sound and viscosity.

The main focus of this research was on fuel type determination using transient rail pressure data to obtain the isentropic bulk modulus of the fuel. The physics behind the bulk modulus formula was studied and observations on pumping quantities with respect to rail pressure were made. The observations were analyzed and conclusions on ΔV were made. It was concluded that the value of ΔV changes with change in rail pressure.

An important step towards bulk modulus estimation is the estimation of pressure rise due to pumping. As pressure rise due to pumping is of prime importance, rail pressure data influenced by pumping only was considered. Pumping intervals of 90°, 180°, 360° were considered to determine an acceptable pumping interval for accurate

ΔP estimation, given the information on engine speed and sampling frequency. The One Moving Window approach was developed to determine the value of ΔP. The approach consists of filtering out noise and oscillations due to rail dynamics and sensors and then estimating the pressure rise. The effect of filter specifications such as pass-band, stop-band edge frequencies and ripples was studied. The frequencies for pass-band and stop-band were calculated based on the signal frequency analysis so as to retain useful frequencies. A detailed signal frequency analysis was done to understand the nature of the transient rail pressure waveform. A Parks McClellan filter was used to filter the rail pressure data. It was concluded that the minimum window size to obtain a good pressure rise estimate could be computed once the pumping duration, filter order, engine speed and sampling frequency are known.

The pressure rise algorithm was first applied to test data for which the accurate pressure rise was known. After determining the parameters to obtain a good estimate of pressure rise, the algorithm was applied to transient rail pressure data from GT-Simulation as well as Cummins rig data. Significant errors, in the range of 0.71% - 2.89%, are seen in the bulk modulus estimates for pressure rise estimates obtained from Cummins test rig data. The difference between biodiesel values for D2 and B100 is 7% [23]. This suggests that the difference between bulk modulus of D2 and B20, which is the blend of biodiesel recommended to be used for transportation [24], is even lower. In order to differentiate between D2 and B20, an error value of 0.1% is desirable. However, the error from bulk modulus estimates in this research does not reach a small enough value required to differentiate between D2 and B20. Apart from this, for bulk modulus estimation, it is necessary to know the pressure dependence on ΔV, which in turn requires knowledge of bulk modulus of the fuel. A possible approach to resolving this issue is by using tangent and secant bulk modulus values and their relationship with each other, to find the values of ΔV and bulk modulus simultaneously from data at several different pressures.

5.2 Contributions

The contributions of this research towards fuel type determination include:

1. Analyzing the bulk modulus formula and demonstrating the effect of rail pressure on pumping characteristics.
2. Integrating the existing GT Models and building a complete system model comprised of the high pressure pump, common rail and six injectors. Modifying this system model to accommodate pumping only with varied pumping intervals.
3. Analyzing the nature of transient rail pressure data by creating test data and confirming the frequency characteristics.
4. Demonstrating the technique of calculating the isentropic bulk modulus for the combined simulation model with pumping only, and a simplified simulation model with pumping only, with various pumping intervals.
5. Developing an algorithm for accurate pressure rise estimation by creating test data.
6. Demonstrating the effect of filter characteristics on rail pressure data through test data.
7. Demonstrating the performance of the bulk modulus estimation algorithm on rail pressure data obtained from GT-simulations as well as a Cummins test rig.

5.3 Recommendations for Future Work

Although the bulk modulus estimation technique does not appear to be a promising technique for fuel type determination through the results obtained in this research, there are several aspects of the technique that need further exploration:

1. The value of ΔV is required in order to calculate the bulk modulus of the fuel. This bulk modulus is the secant bulk modulus and can be written in terms of the tangent bulk modulus. A method to obtain expressions for ΔV in terms of bulk modulus can be developed when collecting data at several different pressures. A possible method of incorporating this is by tuning coefficients to develop the expression for ΔV and solving equations to calculate the values for ΔV and bulk modulus, simultaneously.

2. Other fuel system parameters like sonic speed and density can be further investigated for potential methods for determining the fuel type.

3. Strategies combining multiple parameter estimates can be developed to accurately determine the fuel type.

LIST OF REFERENCES

LIST OF REFERENCES

[1] M. Sakai , D. Yamazaki , T. Akita , N. Kurata. Fuel supply apparatus for internal combustion engine. *U.S. Patent No. 7,007,662 B2*, March 7, 2006.

[2] R. D. Pursifull , G. Surnilla , H. Zhang , M. Meinhart , J. Basmaji. Methods for determining fuel bulk modulus in a high-pressure pump. *U.S. Patent No. 9,243,598 B2*, January 26, 2016.

[3] O. Armas , S. Martinez-Martinez , C. Mata , C. Pacheco. Alternative method for bulk modulus estimation of diesel fuels. *Fuel*, 167:199–207, 2016.

[4] I. Olatunji , N. Clark , P. Sindler , D. McKain , G. Thompson , M. Gautam , S. Wayne , J. Nuszkowski. Biodiesel blend emissions of a 2007 medium heavy duty diesel truck. *SAE Technical Paper 2010-01-1968*, 2010.

[5] A. K. Pandey , M. R. Nandgaonkar. Comparison and evaluation of performance, combustion and emissions of diesel, Jatropha and Karanja oil methyl ester biodiesel in a Military 780 hp CIDI Engine. *SAE Technical Paper 2010-01-2138*, 2010.

[6] US Department of Energy. U.S. biodiesel production, exports and consumption. Energy Efficiency and Renewable Energy, Alternative Fuels Data Center. http://www.afdc.energy.gov/data/10325, 2014.

[7] S. Gupta , V. Manish , D. Gupta , N. Kumar. Comparative study on performance and emission characteristics of fish oil biodiesel and mahua oil biodiesel blend with diesel in a compression ignition engine. *SAE Technical Paper 2013-01-2666*, 2013.

[8] B. He. Advances in emission characteristics of diesel engines using different biodiesel fuels. *Renewable and Sustainable Energy Reviews*, 60:570–586, 2016.

[9] X. Zhang , G. Gao , L. Li , Z. Wu , Z. Hu , J. Deng. Characteristics of Combustion and Emissions in a DI Engine Fueled with Biodiesel Blends from Soybean Oil. *SAE Technical Paper 2009-01-1832*, 2009.

[10] P. Kattwinkel , C. Reith , M. Petersson. Different properties of biodiesel in comparison with standard diesel fuel and their impact on euro vi exhaust aftertreatment systems. *SAE Technical Paper 2012-01-1733*, 2008.

[11] Advanced BioFuels USA. http://advancedbiofuelsusa.info, 507 North Bentz Street, Fredrick, MD, 21701, USA, 2014.

[12] S. Balasubramanian. Fuel type estimation using fuel system parameters. *Master's Thesis, School of Mechanical Engineering, Purdue University*, 2016.

[13] L. Serrano , M. Lopes , N. Pires , L. Ribiero , P. Cascao , L. Tarelho , A. Monteiro , O. Nielsen , M. Gameiro da Silva , C. Borrego. Evaluation on effects of using low biodiesel blends in a euro 5 passenger vehicle equipped with a common-rail diesel engine. *Applied Energy*, (146):230–238, 2015.

[14] B. Nesbitt. *Handbook of Pumps and Pumping*. Elsevier, 2006.

[15] Gamma Technologies. GT-Suite 7.4.0 help documentation on the object 'LookUpFluidProps'.

[16] R. Payri , F. J. Salvador , J. Gimeno , G. Bracho. The effect of temperature and pressure on thermodynamic properties of diesel and biodiesel fuels. *Fuel*, 90(3):1172–1180, 2011.

[17] P.W. Bridgman. *The Physics of High Pressure*. G. Bell and Sons, London, 1958.

[18] Cummins Inc. CCR Fuel System Training Manual. 2014.

[19] J. McClellan , T. Parks. A Personal History of the Parks-McClellan Algorithm. *IEEE Signal Processing Magazine*, 22(2):82–86, 2005.

[20] J. McClellan , T. Parks. Chebyshev approximation for non recursive digital filters with linear phase. *IEEE Trans. Circuit Theory*, 19(2):189–194, 1972.

[21] Purdue University: ECE 438 Digital Signal Processing with Applications. ECE438 - Laboratory 5: Digital Filter Design help documentation. October 6, 2010.

[22] http://www.mathworks.com/help/signal/ug/compensate-for-the-delay-introduced-by-a filter.html. Compensate for the delay introduced by an FIR filter, 2016.

[23] S. Saboo. ME 497 Research Report, Advisor: Prof. Peter Meckl. *School of Mechanical Engineering, Purdue University*, May 2016.

[24] G.Karavalakis , K.Johnson , M.Hajbabaei , T.Durbin. Application of low-level biodiesel blends on heavy-duty (diesel) engines: Feedstock implications on NO_x and particulate emissions. *Fuel*, 181:259–268, 2016.